Mechanical (and Materials) Engineering -- Dissertations, Theses, and Student Research

Mechanical & Materials Engineering, Department of

8-2019

# Design And Evaluation Of Sensor Housing For Atmospheric Boundary Layer Profiling Using Multirotors

Ashraful Islam
*University of Nebraska - Lincoln*, mislam@huskers.unl.edu

DESIGN AND EVALUATION OF SENSOR HOUSING FOR ATMOSPHERIC

BOUNDARY LAYER PROFILING USING MULTIROTORS

by

Ashraful Islam

A THESIS

Presented to the Faculty of

The Graduate College at the University of Nebraska

In Partial Fulfilment of Requirements

For the Degree of Master of Science

Major: Mechanical Engineering and Applied Mechanics

Under the Supervision of Professor Carrick Detweiler

Lincoln, Nebraska

August, 2019

# DESIGN AND EVALUATION OF SENSOR HOUSING FOR ATMOSPHERIC BOUNDARY LAYER PROFILING USING MULTIROTORS

Ashraful Islam, M.S.

University of Nebraska, 2019

Adviser: Carrick Detweiler

Traditional configurations for mounting Temperature–Humidity (TH) sensors on multirotor Unmanned Aerial Systems (UASs) often suffer from insufficient radiation shielding, exposure to mixed and turbulent air from propellers, and inconsistent aspiration while situated in the wake of the UAS. Consequently, atmospheric boundary layer profiles that rely on such configurations are bias-prone and unreliable in descent. This thesis describes the evolution of a novel sensor housing design over three iterations. The sensor housing is designed to shield airborne sensors from artificial heat sources and artificial wet-bulbing while pulling air from *outside* the rotor wash influence. The housing is mounted *above* the propellers to exploit the rotor-induced pressure deficits that passively induce a high-speed laminar airflow to aspirate the sensor consistently. Our design is modular, accommodates a variety of other sensors, and would be compatible with a wide range of commercially available multirotors. Extensive flight tests conducted at three field campaigns with altitudes up to 500 m Above Ground Level (AGL) show that the housing facilitates reliable measurements of the boundary layer phenomena and is invariant in orientation to the ambient wind, even at high vertical/horizontal speeds (up to 5 m/s) for the UAS. A low standard deviation of TH measurements shows a good agreement between the ascent and descent profiles and proves our unique design is reliable for various UAS missions.

COPYRIGHT

© 2019, Ashraful Islam

DEDICATION

To my mother, Afroza Begum, and my wife Rubi Quinones; two powerful women in my life whose continued support helps me survive through all the challenges.

And to my advisor, Dr. Carrick Detweiler, for his patience and continuous support in mentoring me to be a better researcher.

## ACKNOWLEDGMENTS

We thank Jason Finnegan and Amy Guo for their help with data collection during LAPSE-RATE flight campaign. We would like to thank Dr. Sean Waugh, National Severe Storms Laboratory for the radiosonde data. We also thank S. Borenstein and C. Dixon for their help with MURC operations.

## GRANT INFORMATION

# Table of Contents

## List of Figures

**List of Tables**

## Chapter 1

## Introduction

The lower portion of atmosphere up to 1.5 km Above Ground Level (AGL) is called Atmospheric Boundary Layer (ABL). High-resolution profiles of the ABL are critical for obtaining measurements important for a range of microscale and mesoscale phenomena. Observations of atmospheric parameters in ABL enables weather forecasting, numeric weather prediction, severe-weather predictions, climate change research etc. These profile measurements are conventionally performed using ground-based balloon launches [17, 38] and parachute-based dropsondes [16]. However, these methods are insufficient for targeted and controlled ABL research and lack spatial and temporal resolution for detection of micro-scale changes in atmosphere.

Recent technological advancements have enabled the use of Unmanned Aerial Systems (UASs) to perform targeted, controlled, and frequent profiles using fixed wings [10] and multirotors [4, 18]. Both fixed-wing and multirotor UASs offer distinct advantages over passive balloon and parachute systems in terms of the ease, frequency, and spatiotemporal resolution of observations. More specifically, multirotors have flight profiles that allow easy operation, a geometry that offers convenient placement for a variety of sensors, and a payload capacity that even permits heavier sensors (ultrasonic anemometer, particle counter, aerosol sensor,

etc.) to be airborne. Furthermore, their relatively small launch/land footprint makes them suitable for use in remote locations without the need for runways [24]. As a result, their use for a variety of profiling applications such as the measurement of Temperature–Humidity (TH) data [6, 12], wind-estimation [35, 34, 33, 31], air quality measurements [40, 41], etc. has increased significantly in recent years.

This thesis develops the housing for TH measurement, which is shown mounted and fully assembled on a multirotor in Figure 1.1. This housing outperforms traditional mounting configurations for TH sensors (underneath the body, under the propeller-arm, etc. described in Section 3.2, and Table 3.1) in terms of data consistency, correctness, and reliability. The performance improvements of the housing come from mitigating three primary sources of measurement errors of a TH sensor mounted on a multirotor:

- Error/uncertainty due to sensor response time.

- Measurement error due to solar radiation (insolation).

- Undesirable mixing of sample air.

This mitigation is the result of pulling air through the housing sourced away from UAS-disturbed airflow while maintaining a high airflow speed. Furthermore, the modular and light-weight design makes it convenient to set up in the field and adaptable to a range of UASs and sensors. The housing system imposes minimal constraints on regular flight operations.

Obtaining a precise air temperature is particularly challenging as uncertainties can arise from multiple sources such as the diameter of the sensor, the airflow speed for aspiration, the sensor self-heating, the sensor response time, etc. [8, 9]. Additionally, undesired mixing in the air, such as that of the propeller flow field,
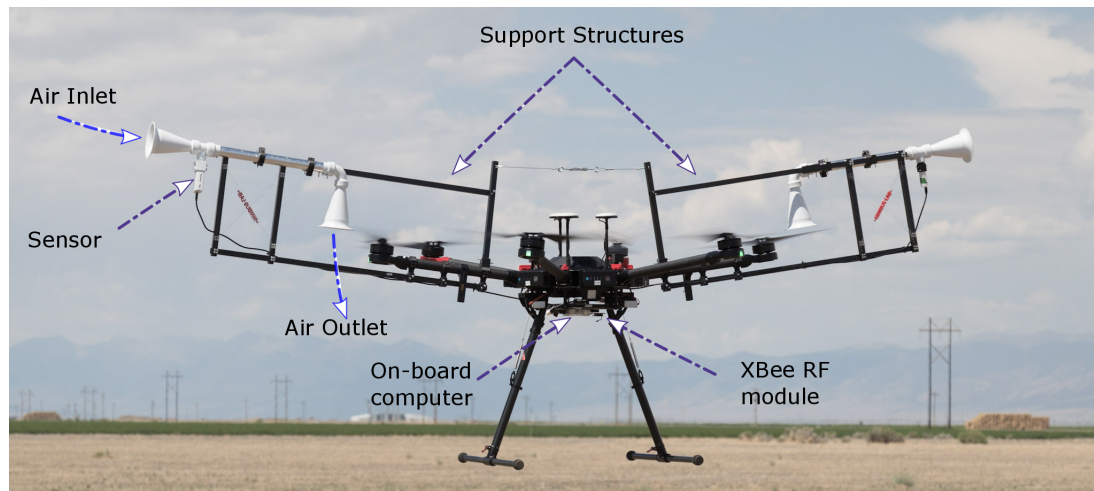
Figure 1.1: A field trial of sensor housings mounted on a *DJI M600 Pro* UAS using the square carbon-fiber tube support structure.

can cause a misrepresentation of the observation level or an undesired smoothing of atmospheric features. As a result, the quality of the measurements made by the sensor is also extremely dependent on its placement on the UAS's body [14, 23] and aspiration speed [19]. TH sensors are particularly sensitive to a lack of aspiration and inadequate shielding from insolation and precipitation, the latter of which can cause erroneous wet-bulbing. A TH sensor mounted underneath the rotor of the multirotor, for example, can introduce bias into its measurements due to insolation, compressional, and frictional heating [14, 13]. The sensor will also have inconsistent aspiration due to rotor turbulence [39, 43]. Moreover, because the air beneath the rotors originates from the area above the aircraft, observations using traditional mounting have uncertainty in the actual observation level. These biases are particularly acute in descent profiles, making it extremely difficult to ensure the minimum vertical resolution to accurately capture atmospheric phenomena [15].

Consequently, several TH-measurement approaches rely only on the ascent data [27, 26, 15] while using only minimal measures to shield the sensor. Ideally, placing the sensor farther away from the body of the UAS increases the validity

of the recorded observations [41]. Although many different probes for air/gas parameter measurement exist where the flow is sucked inside a tube [5]; our method does not rely on vacuum pump/atmospheric wind to induce the flow. We use an expander-reducer strategy to exploit the low-pressure region on top of the propeller to induce a high-speed flow that satisfies the requirements of TH sensors. However, doing so requires a careful design of a sensor housing that fulfills all the requirements of sensors and UAS and still maintains reasonable margins of safety for UAS flight operations.

In this thesis, we present a novel housing design for mounting TH sensors that not only ensures environmental shielding but also provides consistent aspiration throughout the mission despite the changes in airflow field around the UAS. Our design innovation ensures that measurements are taken from the air far away from the body of the aircraft and near the actual observation level. The housing passively uses the suction induced by the propellers to create a high-speed laminar flow inside the sensor housing tube.

We present our results from various field deployments in Oklahoma, Nebraska and Colorado, USA. Our evaluations focus on three fundamental contributions of the design: (1) reliable temperature–humidity sensor readings during both ascent *and* descent in vertical profiling missions at varying speeds; (2) invariance of the orientation of the housed sensors to ambient wind (or lack thereof); and (3) the ability to capture atmospheric phenomena (such as an inversion layer) when compared to a radiosonde. We note that, although wind measurement is one of the parameters of interest in ABL studies, our sensor housing is not designed for atmospheric wind measurement. Our primary research goal is acquiring accurate temperature-humidity measurements using the proposed sensor housing. However, based on the findings of the thesis, we have noted the importance of

on-board wind measurements in the discussion of future work.

The rest of this thesis is organized as follows: Related Works are discussed in Chapter 2, Chapter 3 details the requirement of the system and the designed system, Chapter 4 discusses the evolution of the sensor housing with detailed description of each stage, Materials and Methods to evaluate the sensor housings are presented in Chapter 5. In Chapter 6, the Results are presented, followed by a Discussion of the results in Chapter 7 and the Conclusion in Chapter 8.

## 1.1   Contributions

Parts of this thesis is published in [20, 23], where we investigated two new sensor housing configuration and one traditional multirotor sensor mounting method. We participated in two flight campaigns (Appendix A.3): Stillwater, Oklahoma, 2018, and Wilber, Nebraska, 2018- to evaluate those three sensor housing configurations.

Also, in parts of this thesis published in [22] we evaluated an improved housing configuration. We participated in a six day long flight campaign in San Luis Valley, Colorado, to evaluate the performance of this sensor housing. The field campaign is named Lower Atmospheric Process Studies at Elevation—a Remotely-piloted Aircraft Team Experiment (LAPSE-RATE) flight campaign conducted as part of the 2018 annual meeting of the International Society for Atmospheric Research using Remotely-piloted Aircraft (ISARRA) [21]. Based on the results from this field campaign, further optimization on the design is made to improve UAS flight stability.

In summary, over three iterations of the design, we developed and field-tested a sensor housing for TH sensors that:

- Has consistent airflow to facilitate fast and consistent sensor response time.

- Has low thermal mass and better radiation shielding to reduce radiation error and sensor housing response time constant.

- Samples air from a source far removed from UAS turbulence and undesired mixing.

- Is independent of orientation relative to wind or sun.

- Provides reliably consistent measurement in both UAS ascent and descent.

- Protects the sensor from artificial heat sources and prevents artificial wet-bulbing.

- Has foldable, modular design for fast field deployment and easy replacement.

- Is compatible with other sensors with aspiration requirements similar to TH sensors.

# Chapter 2

# Related Work

TH sensors are particularly sensitive to their placement environments. Despite having the advantages discussed in the introduction, the airflow field of a multirotor can interfere with reliable measurements of atmospheric phenomena. Sensor housing design needs to consider the requirements of TH sensors, sensor housing requirements, and the flow field of UAS.

Prior works on characteristic considerations of TH sensors are discussed in Section 2.1, considerations for sensor housing and its performance criteria are discussed in Section 2.2, flow field characteristics of a multirotor which will affect the performance of both TH sensors and the housing is discussed in Section 2.3, and the chapter concludes with a discussion of the current state of the art and challenges in Section 2.4.

## 2.1 Considerations for TH Sensors

### 2.1.1 Response Time

Accurate measurement from temperature sensors is crucial for detection of atmospheric phenomena. Performance of such sensors are primarily dependent on the placement environment and can pose significant challenges to data correc-

tion/processing if all the requirements are not met. Rodi and Spyers-Duran [37] describe that the ability of the sensors to respond to rapid change in temperature is dependent on the sensors, as well as the thermal mass of the housing, and housing flow condition. McCarthy [29] describes a method for correcting the response of temperature sensors for system response time. According to McCarthy, response time of the system should be determined as flown to account for the response lag of the housing and the sensor itself. Sensor response is also dependent on the speed of the aspirating airflow. Houston and Keeler [19] show the impact of airflow speed on the sensor response time. Sensors in a high aspirating flow respond faster compared to low aspirating airflow. If the airflow is not consistent, this can be very hard to take into account when correcting for sensor response time.

### 2.1.2 Source of TH Measurement Errors

Podesta *et al.* [8, 9] describes the challenges in precision meteorology: radiation error, sensor self-heating, sensor response time correction. According to Podesta, the magnitude of radiation error is dependent on the sensor diameter; with small diameter sensors having the lowest error. Although most of the modern precision temperature sensors have a small diameter, adding radiation shielding is still critical to minimize the radiation error.

Sensor self-heating is another factor that can introduce error in the measurement. Without sufficient aspiration, the effect of sensor self-heating will be significant and can be hard to correct in post-processing. Artificial heat sources such as motor waste heat as hypothesized by Greene *et al.* [14] can also introduce bias in the measurement. According to their experiments, bias can be a few times the specified accuracy of the sensors. Since the artificial heat sources are not consistent

Table 2.1: Desired accuracy of TH sensors [23].

| Sensor | Desired Accuracy |
| --- | --- |
| Temperature | $\pm 0.2\,^{\circ}C$ |
| Humidity | $\pm 5.0\,\%RH$ |

throughout the flight and fluctuate, they can not be calculated or taken into account by prior experiments.

TH sensors thus need to be placed in a way that minimizes the sources of error and thus the steps taken in post-processing to improve the quality of the TH data.

## 2.2   Considerations for Sensor Housing

Sensor housing must be designed to meet accuracy/precision requirements for atmospheric missions and must consider the restrictions set forth by the environment, sensors, and UAS. Jacob *et al.* [23] discussed considerations for atmospheric measurement using UAS focusing on the observed sensor response, and the effect of orientation of the UAS. According to [23], observed sensor response during descent is slower than that of ascent and does not pick up fine-scale changes accurately.  Data from a previous version of the sensor housing (discussed in chapter 5) shows the dependency on the orientation of the sensor housing related to the atmospheric wind, where if the sensor housing inlet is pointed downwind the sensor suffers aspiration issues. Jacob *et al.* also discusses the desired accuracy of TH sensors as shown in Table 2.1

The issue with UAS descent data being unreliable with the traditional mounting method is also noted by Lee *et al.* [26, 27] as he describes uncertainty in UAS sensor measurements during descent. Following this, many authors [26, 27, 15] discard the descent data altogether.  Since descent is almost half the flight time, and

multirotors are known to have very limited battery capacity, current methods of sensor placements are ineffective and inefficient. A sensor housing that allows the use of both ascent and descent data would significantly increase the amount of data collected with better spatiotemporal resolution.

Greene *et al.* [14] compared temperature sensor performance for multirotors at various placement locations along the arm between two extremities of the rotor. The sensor they tested had a radiation shield and was passively aspirated by the UAS airflow field. Their experiment shows that the sensors are not properly aspirated ($\ll 5\,\mathrm{m/s}$) directly underneath the motor and at the center of the UAS. Sensors also show warm bias up to a degree Celsius directly underneath motors and up to 0.3 degree Celsius at the center. Another key observation is that at high aspirating airflow, sensors read values closer to the reference temperature, and absence of aspiration causes sensors to show gradual warming drift likely due to self-heating of the UAS and radiation shielding. Green *et al.* concluded sensors placed underneath the propeller 2/3 propeller radius away from the motor is optimum among the compared methods. However, the study did not consider/compare placements on top of the propeller or away from the UAS body.

Hemingway *et al.* [15] used experimental data to determine vertical sampling scales for UAS to capture the thermodynamic structure of atmospheric phenomena (such as temperature, humidity). The recommended vertical sampling scale for temperature is $3\,\mathrm{m}$ and humidity is $1.5\,\mathrm{m}$. However, sensor placement location for this experiment (center of the UAS) is not recommended [14], and only one ascent speed is used (about $2\,\mathrm{m/s}$) in the experiments. Furthermore, the reliability of the experimental data is not established against any ground truth or comparable measurements. Effect of sensor response time and ascent speed is not considered either.

Houston and Keeler [19] showed how sensor response and airspeed affect the representation of a couple of common atmospheric phenomena from UAS measured values. It is shown that the difference between ascent and actual profile increases with sensor response time but decreases with airspeed. Increased ascent speed also increases the error. Another important observation from the result is that an increase in sensor response time causes unwanted smoothing of the observed data and will seem to be lagging behind the original data.

According to findings of Villa *et al.* [41], air pollution measurements are more accurate as far away from the UAS center as possible as UAS causes a 'dispersion' effect and lowers the concentration measurement. The consideration of this effect is essential for many sensors that rely on concentration measurement. For example, if a humidity sensor relies on the moisture content of the air for accurate measurement, mounting it in the turbulent field of UAS would give unreliable measurements. They also note that mounting sensors farther away also adversely affects the sensor response time, as the airflow on the sensor is very low in the absence of prop wash. However, mounting a sensor further away would require careful design of a sensor housing that maintains the aspiration.

Another important consideration for traditional sensor mounting for multirotor is the shielding from radiation. The radiative error can lead to measurement errors up to a few degrees Celsius [2] which can be worse in the absence of sufficient aspiration.

## 2.3 Multirotor UAS flow field

Prudden *et al.* [34] measured rotor interference in a wind tunnel as a function of rotor diameter in a simulated forward flight, and found the effect to be very

minimal at 2.7x rotor diameter away from the motor when the sensor is directly facing the incoming wind. However, this experiment does not verify sensors situated downstream of the UAS.

Yoon *et al.* [43] and Ventura *et al.* [39] conducted extensive CFD simulation of multirotor to visualize the aerodynamic field around the UAS. Based on the simulation result, it can be seen that in the absence of wind, a sensor just outside the UAS rotor would experience little to no turbulence. This finding agrees with earlier literature from Villa *et al.* [41] in which authors experimentally measure the wind field around the hexacopter at different measurement points. However, in practice, the absence of wind is rarely the case; either the wind or lateral movement of UAS would carry the disturbed airflow further downstream. A sensor mounted downstream will be affected unless it is very far from the body, which may make it structurally challenging to implement. Given the knowledge of aerodynamics of the airflow, a sensor housing mounted on top of the UAS with inlet further out will be interfered the least when it is downstream.

## 2.4 Current State of the Art and Challenges

Lee *et al.* [28] shows how the multirotor and other UASs can augment the radiosonde data collected in lower ABL (up to 1.5 km AGL). Lee also discusses the importance of assimilating fixed wing and multirotor UAS data for weather models to improve forecasting.

Barbieri *et al.* [3] describes the challenges faced in comparing sensor data from different UAS platforms. Currently, data collected using UAS does not have any standardized mounting methods for multirotors, resulting in huge variations among the data collected [3].

Our recent paper [22] describes the challenges of the multirotor TH measurement, and the effectiveness of sensor housing, described in this thesis, in reducing measurement uncertainties. This thesis extends the work on the sensor housing further with improved design focusing on UAS stability.

**Chapter 3**

**Requirements and Description of the System**

This chapter describes the design requirements set forth by the sensors and the UAS in Section 3.1, evaluation of sensor placement configurations that have been considered in this thesis is detailed in Section 3.2, and the details of the system description along with the specifications for the sensors and platform configurations during field campaigns are described in Section 3.3.

## 3.1  Design Requirements

The design of a sensor housing system has several fundamental requirements that stem from the properties of the sensor and the flight characteristics of the UAS.

**Requirements of the Sensor:** TH sensors require sufficient aspiration, protection from external heat sources (such as insolation and UAS waste heat), and prevention of artificial wet-bulbing.

- *Aspirating Sensors:* Naturally aspirated sensors are prone to radiative heating error [2]. The aspiration airspeed also affects the effective sensor response times [19]. Insufficient and inconsistent aspiration speeds introduce uncertainty in the measurement that could be impossible to deal with during quality checks/correction of the data. Sensor manufacturers often specify the sensor

response time in the presence of constant airflow. For instance, a nominal 5 m/s airflow is used for the response time of 1 s for iMet sensors (Table 3.2). However, when mounted on a system, the response time of the *system* could change based on the aspiration method and should be determined *as flown* [29].

- *Shielding from Heat Sources:* The sensors need to be protected from solar radiation and other heat sources such as the waste heat produced by the battery and motors and absorbed heat from solar radiation by the body of the UAS. Failure to do so will result in biased measurements, which can worsen the longer a UAS-mounted sensor is airborne. Having a sufficiently aspirated housing and proper placement of the sensor will reduce/eliminate the effect of these biases.

- *Preventing Artificial Wet-Bulbing:* The sensor housing needs to shield the sensor from precipitation and should not allow water to accumulate on the sensors. The accumulation of liquid water on the sensor can produce incorrect measurements of the temperature by the wet-bulbing effect. If the humidity sensor package is dependent on the temperature sensor for corrections, this will also skew the humidity measurements by an undesired saturation.

**Requirements of the UAS:** The general requirements from the perspective of the UAS are that the weight and size of the housing must be within the bounds of the UAS's payload capacity. At the same time, the placement of the housing must not hinder safe and normal operations of the UAS.

- *Payload Capacity:* The sensor housing and its mounting fixtures must not exceed the rated payload capacity of the aircraft. A higher payload weight

also reduces the total flight time, thereby limiting the type of mission the UAS will be capable of performing.

- *Flight Dynamics:* The housing must not prevent the UAS from doing its normal maneuvers and must remain in safe operating conditions. Adding the sensor housing must not severely disrupt the balance of the UAS.

## 3.2  Evaluation of Sensor Placement Configurations on the UAS

The different sensor configurations considered in the thesis are shown in Figure 3.1 and summarized in Table 3.1. One approach to placing the sensor would be to mount it directly underneath the propeller (configuration 1) to meet the aspiration requirements, but the flow field of a propeller is turbulent [39, 43] and the resulting aspiration is unsteady. Sensors in this configuration can show bias due to frictional and compression heating by propellers and motor waste heat [14, 13]. Also, airflow passing across the sensor originates from a large area above the UAS [39], making the location of actual measurements uncertain. Alternatively, the sensor can be placed on top of a propeller (configuration 4) where the air is relatively unmixed, and the flow is comparatively laminar. However, as the UAS descends into turbulent and mixed air created by its propeller, this sensor configuration will be in the wake of the UAS, will be measuring data from an uncertain/mixed source, and will potentially experience uncertain aspiration if obstructed by the UAS body. Moreover, the resulting aspiration might be insufficient and unreliable as the airflow speed is dependent on the propeller dimension and relative distance from the motor.

Another popular mounting method is configuration 2, as seen in [26]. Insufficient aspiration is also a potential issue if the UAS is to be used in a similar config-
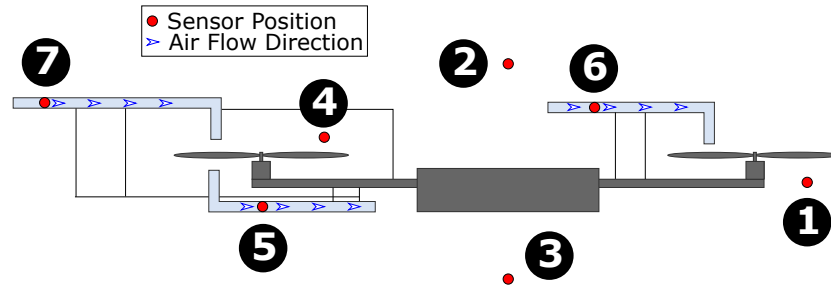
Figure 3.1: A schematic of the different Sensor Placement Configurations: **1** Direct Downwash, **2** Over the UAS, **3** Under the UAS, **4** Direct Upwash, **5** Downwash housing, **6** Upwash Housing with Inlet Pointed Inside, and **7** Upwash Housing with Inlet Pointed Outside.

Table 3.1: A comparison of the different sensor configurations: ✓ the availability of aspiration for temperature–humidity (TH) and atmospheric shielding.

| No. | Configuration | Temperature | Humidity | Shielding | Comments |
|-----|---------------|-------------|----------|-----------|----------|
| 1 | Direct Downwash | ✓ | ✓ | x | Mixed air; reading is especially unstable during descent |
| 2 | Over the UAS | x | x | x | Insufficient aspiration |
| 3 | Under the UAS | x | x | x | Mixed air and insufficient aspiration |
| 4 | Direct Upwash | ✓ | ✓ | x | Possibly insufficient aspiration |
| 5 | Downwash housing | ✓ | ✓ | ✓ | Mixed and turbulent Air |
| 6 | Upwash Housing with Inlet Pointed Inside | ✓ | ✓ | ✓ | Air source is in the wake of the UAS |
| 7 | Upwash Housing with Inlet Pointed Outside | ✓ | ✓ | ✓ | Air is sourced outside of the UAS interference |

uration as a radiosonde-weather-balloon where the sensor is passively mounted above or hanging from the UAS (configurations 2 and 3), as the airflow speed decreases drastically towards the center of the UAS [41]. Any sensor mounted outside of the housing (configurations 1–4) due to the lack of shielding also runs the risk of bias from insolation or erroneous wet-bulbing. The sensor mounted inside a horizontal cylinder in configurations 2 and 4 could provide radiation shielding and, in some cases, provide sufficient aspiration (only if the atmospheric wind speed/horizontal velocity of the UAS is high and in a specific orientation), but this will limit the use case of the multirotor in ABL measurements. Both of the

configurations will still be in the wake of the UAS during descent, hence adding uncertainty to the observations during descent.

Sensors inside the housing, as shown in Figure 3.1 (corresponding to configurations 5–7), will be shielded from radiation and would maintain sufficient aspiration. Configuration 5 will have turbulent air and potential aspiration issues during descent. Configuration 6 (even though it is better than configuration 5) could be subjected to waste heat of the UAS body, and its air source will be in the wake of UAS during descent. Considering an extensive evaluation of configurations 1–6 in our previous effort [23, 20], along with the fact that a sensor placed in configuration 7 will sample the air that is significantly less interfered by the UAS, configuration 7 would be the best choice.

Aspirating air flow through the housing could be induced using active or passive air draw. The active draw of air will require additional hardware like a fan, a battery, and associated electronics [13]. This also does not utilize what is already available in a UAS, i.e., the wind field from the propellers. Additional hardware will also make the housing heavier and will reduce the flight time of the UAS. Using the propeller of the UAS to draw air passively can facilitate a similar (or better) performance with less payload.

Since for the housing in configuration 7 the air source is far from the center of a multirotor, the extension has the potential to compromise the stability of the UAS by introducing an extra moment on one arm. To balance the moment, we choose to mount a second housing in a symmetric configuration on the opposite arm. We note that this may make the UAS less responsive to control inputs in the roll/pitch axis.

Based on the above design considerations, this thesis uses symmetric configuration 7 for sensor housing (with passive air draw), as seen in Figure 1.1. As for

comparison against sensors without sensor housing, we choose configuration 3.

## 3.3 System Description

The primary components of the housing system, as shown in Figure 1.1, are the UAS, Data Acquisition System (DAQ), sensors, sensor housing, and support structure for sensor housing.

**UAS:** The UAS configuration is a "DJI Matrice 600 Pro" hexacopter platform equipped with a "DJI A3 Pro" flight control system. The dimensions of the system are 1668 mm × 1518 mm × 727 mm with propellers, frame arms, and a GPS mount unfolded (including landing gear). The maximum takeoff weight of the UAS is 15.5 kg (the maximum recommended payload is 5.5 kg) with a flight endurance of 35–40 min on a single set of six "DJI TB48S" batteries with no load. The manufacturer specified positioning accuracy is vertically ±0.5 m and horizontally ±1.5 m [1]. The maximum ascent and descent speeds are 5 m/s and 3 m/s respectively.

**DAQ:** All the experimental data are obtained and recorded onboard the UAS by an Odroid XU4 [32], which is a compact single-board computer with eight processing cores and 2 GB of RAM. The Odroid runs a Robot Operating System (ROS) [36] node that communicates with the autopilot on the UAS to collect the position, velocity, altitude, attitude, and other control information. It also interfaces with the TH sensors to obtain temperature and humidity measurements. Different ROS nodes collect data independently of each other and record the timestamp of when the ROS node collected the data and when the ROS core received the data, which simplifies the synchronization between the different sources of data nodes. A wireless serial interface to the Odroid (over 2.4 GHz Xbee radios) allows two-way communication from a ground station, which is also useful for debugging and

periodic sanity checks. The raw data file, recorded by the ROS, is retrieved over an ethernet connection and post-processed in MATLAB.

**Sensors:** Detailed specifications of the TH sensors used in the thesis are described in Table 3.2. The primary sensors used for the experiments are iMet XQ2 and iMet XQ1 from InterMet Systems (Grand Rapids, MI, USA). InterMet sensors feature a self-contained sensor package designed for UASs that include atmospheric pressure, temperature, and humidity sensors. These sensor units also have built-in GPS and an internal data logger with a rechargeable battery.

Additionally, a custom two-node sensor, called `nimbus-pth`, designed and built in our lab, was mounted on one of the UAS platforms. The `nimbus-pth` sensor has a high precision thermistor configured in a Wheatstone bridge and is read by a 10-bit analog-to-digital converter. The humidity sensor is an "SHT31" sensor, while the pressure sensor is an "MS5803" sensor. For experiments involving measurements of airflow speed inside the housing, a hot wire thermo-anemometer "Extech SDL350" is used inside the housing. The anemometer has a specified range of 0.2–25 m/s with a resolution of 0.01 m/s and accuracy of 5% of the reading.

The first ground truth reference used for the experiments is the instrumented van of Colorado University, Boulder, CO named MURC (Mobile UAS Research Collaboratory) [30]. As part of the LAPSE-RATE'2018 flight campaign intercomparison of multirotor and fixed wing platforms, 13 institutions and organizations used the measurement from the MURC tower as the ground truth to fly 35 UASs in a similar flight pattern. The MURC has a 15.2 m extendable tower that is equipped with Gill MetPak Pro Pressure, Temperature, Humidity (PTH) sensors. The MetPak Pro sensor has a manufacturer-specified accuracy of ($\pm$0.1 °C) for temperature and ($\pm$0.8% of RH) for humidity. The filtering process of MURC sensors are proprietary

Table 3.2: The key specifications for the sensors used in different experiments: The unavailable fields are left blank.

| | | XQ2 (iMet XQ2) | XQ1 (iMet XQ1) | nimbus-pth (Custom Built) | MURC (Gill MetPak Pro) | RadioSonde (RS92) |
|---|---|---|---|---|---|---|
| Temperature | Type | Bead Thermistor | Bead Thermistor | Bead Thermistor | pt100 1/3 Class B | Capacitive Wire |
| | Range | −90 to 50 °C | −95 to 50 °C | −40 to 100 °C | −50 to 100 °C | −90 to 60 °C |
| | Response Time | 1s @ 5 m/s | 2 s | 1 s | <0.5 s | <0.4 s @ 6 m/s flow |
| | Resolution | 0.01 °C | 0.01 °C | 0.01 °C | 0.1 °C | 0.01 °C |
| | Accuracy | ±0.3 °C | ±0.3 °C | | ±0.1 °C | 0.5 °C |
| Humidity | Type | Capacitive | Capacitive | Capacitive | | Capacitive |
| | Range | 0–100% RH | 0–100% RH | 0–100% | 0–100% RH | 0–100% RH |
| | Response Time | @ 25 °C, 0.6 s @ 5 °C, 5.2 s @ −10 °C, 10.9 s | 5 s @ 1 m/s velocity | 8 s | | @ 20 °C, <0.5 s @ −40 °C, <20 s @ 6 m/s |
| | Resolution | 0.1% RH | 0.7% RH | 0.01% RH | 0.1% RH | 1% RH |
| | Accuracy | ±5% RH | ±5% RH | ±2% | ±0.8% | 5% RH |

by the manufacturer and not available.

Another ground truth used in this thesis is radiosonde balloon observation data provided by the National Oceanic and Atmospheric Administration (NOAA). The balloons were deployed by NOAA officials close to the UAS launching site by following standard deployment guidelines. The sensor used in the radiosonde is Vaisala RS92 (Vaisala Corporation, Vantaa, Finland) with a very fast response time for both temperature (<0.4 s) and humidity(<0.5 s). The radiosonde data presented in the thesis is corrected and filtered for sensor response lag and other factors by proprietary Vaisala algorithms.

## 3.4 UAS Sensor Mounting Configuration and Payload

Mounting configurations of the sensors and UAS platforms for the three flight campaigns are described in this section.

**Oklahoma'2018:**

During CLOUDMAP flight campaign of Oklahoma, one multirotor UAS platform (Matrice 600 Pro) is used with three sensor configurations - direct downwash (configuration 1), downwash housing (configuration 5), downwash housing with

inlet pointed inside (configuration 6).

Sensors for all three configurations were iMet XQ1 sensors described in the previous section.

**Nebraska'2017:**

Total solar eclipse campaign featured two sensor configurations with two sensors in configuration 1 and one sensor in configuration 5.

Sensors for all three configurations were iMet XQ1 sensors described in the previous section.

**LAPSE-RATE'2018:**

The sensor mounting configuration of the sensors is referred to as a configuration number, as described in Section 3.2 and Figure 3.1. The placement configuration of the sensors used in the experiments for each of the UAS is as follows:

*UAS platform M600P1*: one XQ2 (code name: P1XQ2) is mounted inside the left sensor housing (configuration 7), and one XQ1 (code name: P1XQ1) is mounted inside the right sensor housing (configuration 7). The alternative setup used in some experiments replaces XQ1 with `nimbus-pth` (code name: P1Nimbus2) inside the housing. An additional `nimbus-pth` (code name: P1Nimbus1) is also placed under the body of the UAS without housing (configuration 3).

*UAS platform M600P2*: one XQ2 (code name: P2XQ2) is mounted inside the left sensor housing (configuration 7), one `nimbus-pth` (code name: P2Nimbus2) is mounted inside the right sensor housing (configuration 7), and an additional `nimbus-pth` (code name: P2Nimbus1) is placed under the body of the UAS without housing (configuration 3).

This form of sensor placement facilitates an evaluation between the sensor placed inside the housing (configuration 7), as shown in Figure 3.2a, versus under the body of the UAS without housing (configuration 3), as displayed in Figure 3.2b.

(a) TH sensor inside the housing


(b) TH sensor under the UAS body without housing

Figure 3.2: The sensor configurations used in the experiments for this thesis: The sensor without housing is mounted without any additional radiation shielding.

For the configuration used in the experiments, the UAS's payload was ~1.8 kg (housing with support structure and sensor—2× ~720 gm, onboard computer—140 gm, misc cables, screws etc.—approx. 200 gm) with a flight endurance of 20–25 min, which makes it capable of vertical profiling missions up to 1000 m AGL at 2 m/s.

# Chapter 4

## Sensor Housing Design

Our work on sensor housing has evolved over three iterations, where we improved the sensor housing to be more reliable and suitable for a greater range of applications related to atmospheric science. Figure 4.1 shows the evolution of the sensor housing over three iterations. Section 4.1, 4.2 4.3 describes the housing with detailed schematic for first, second and third iteration respectively. Each section concludes with the overview of design goals and lessons learned.

In our first iteration, the design goals were to house the sensor with readily available cheap materials with the least burden on the UAS flight. We learned which configuration works better and identified the issues: the source of air needs to be outside the UAS interference, air flow speed inside the housing needs to be higher for indirect air draw using upwash. The best configuration found in the first iteration was found to be configuration 6 (Section 3.2) that uses the indirect draw of air to avoid mixing of air inside the housing.

The second iteration was focused on extending the housing outside the UAS interference and increase the airflow. Inlet and outlet were chosen to be reducer and expander configuration such that a very high-speed flow is achieved inside the housing with laminar airflow at the inlet. Light materials were chosen to keep the weight of the housing as low as possible to minimize the moment exerted on

(a) Version 1
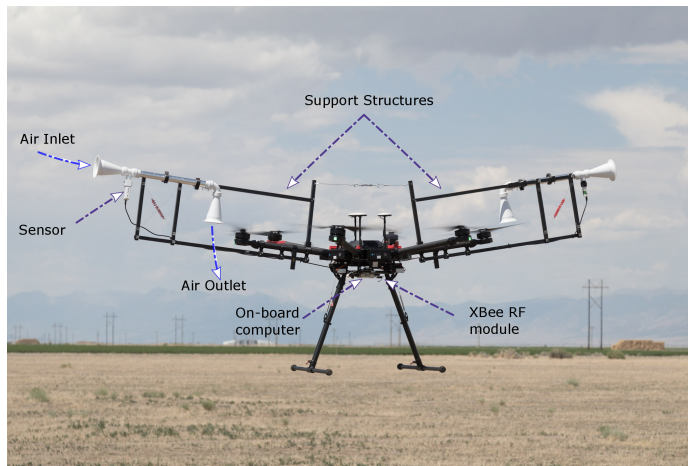


(b) Version 2



(c) Version 3

Figure 4.1: Evolution of Sensor Housing

the UAS during flight. The sensor readings from this iteration of housing have been phenomenal, allowing the data from both ascent and descent to be useful. Since the housing was extended outside the UAS body, it tends to add disturbance to UAS controls when flying through a turbulent region of the air.

The third iteration focuses on improving the UAS flight stability by optimizing the mounting of the housing in terms of weight and symmetry. Additionally, the foldability and easy mounting of the housing improves transportability and deployability. Since the overall weight of the payload is significantly less, the flight time of the UAS is expected to increase as well.

## 4.1 Sensor Housing: First iteration

During the first stage of the development of the sensor housing as shown in Figure 4.2, three placement configurations were selected: direct downwash (configuration 1), downwash housing (configuration 5), and upwash housing (configuration 6). Sensor housing configurations are described in Table 3.1.

*First* type of housing is the direct downwash (configuration 1); this is one of the widely used traditional mounting methods [14]. A schematic of the mounting is shown in Figure 4.3a. This housing is designed to be mounted directly on the arm to expose the sensor in the propeller wash for aspiration. Since the sensor does not have any radiation shield in this configuration, the housing is split into three components to enable 2-DoF rotation such that angle of the sensor could be adjusted before flights as to minimize the incident solar radiation.

*Second* type of housing used in the first iteration is downwash housing (configuration 5). The housing is built using cheap and readily available 1-inch PVC tubes and elbow bend. Sensors inside the housing are mounted using 3D printed
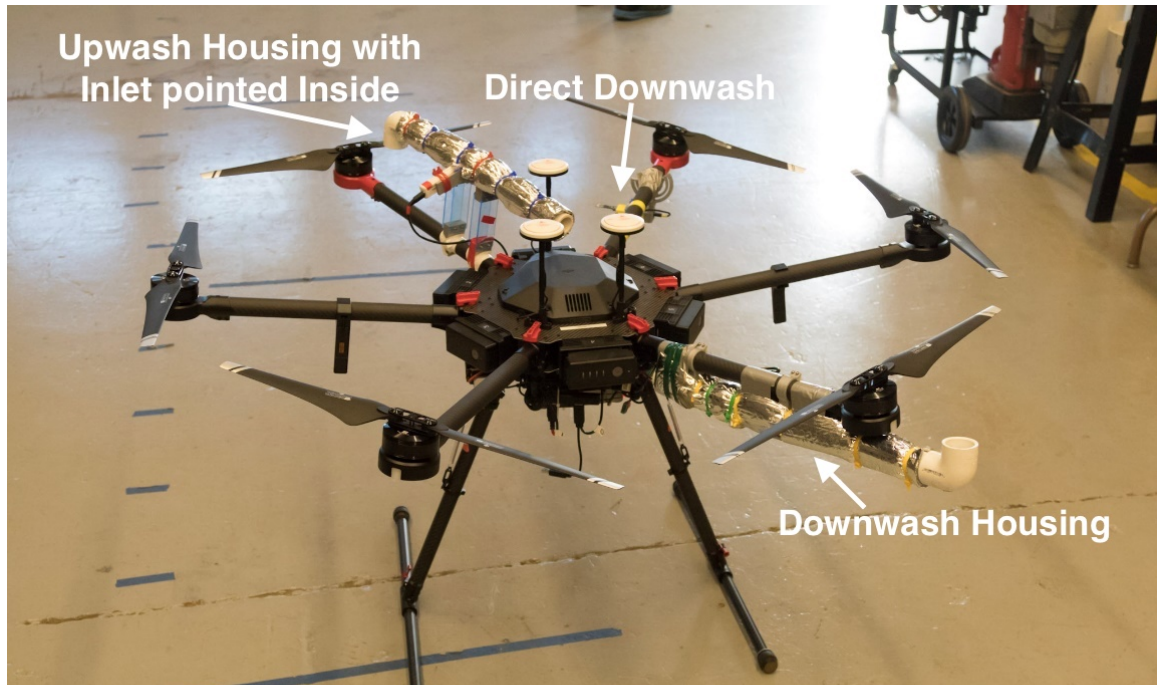
Figure 4.2: Sensor housings: first iteration

mountings, as shown in Figure 4.3a. Highly reflective bubble wrap is used to shield against solar radiation.

*Third* type of housing is upwash housing with inlet pointed inside (configuration 6). It should be noted that configuration 5 and configuration 6 are identically built but mirrored in terms of placement about the UAS center. As such, what is an inlet of the downwash housing would be the outlet of the upwash housing. This sensor housing poses challenges when mounting to arms as there is an additional moment acting on the joint. However, this configuration draws a laminar airflow through the sensor and is anticipated to produce more stable sensor readings.

Based on the experiments using the first iteration of housing, we learned that: source of air inside the UAS interference can cause fluctuations in the reading, air flow speed inside the housing needs to be higher and more consistent to provide reliable response time, airflow inside the downwash housing is possibly turbulent
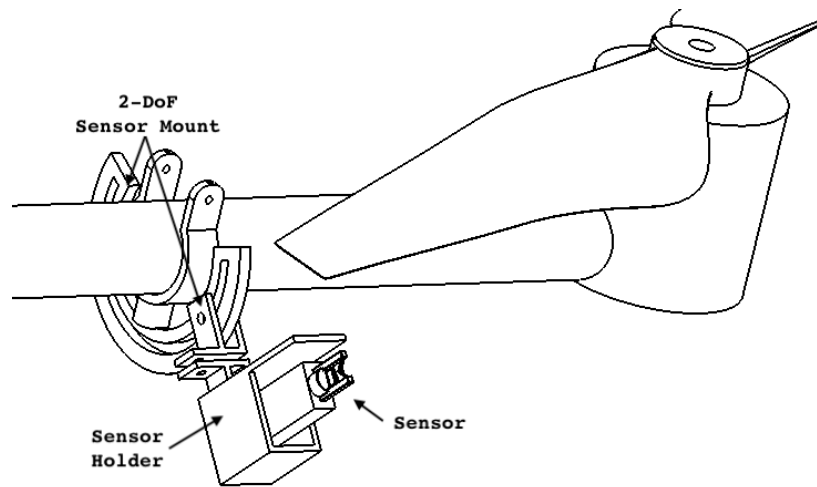
(a) Direct downwash housing schematic
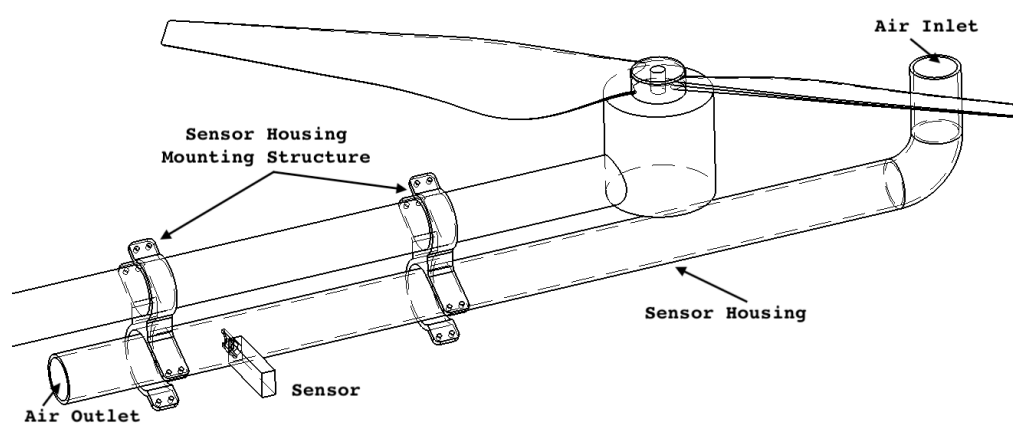


(b) Downwash housing schematic
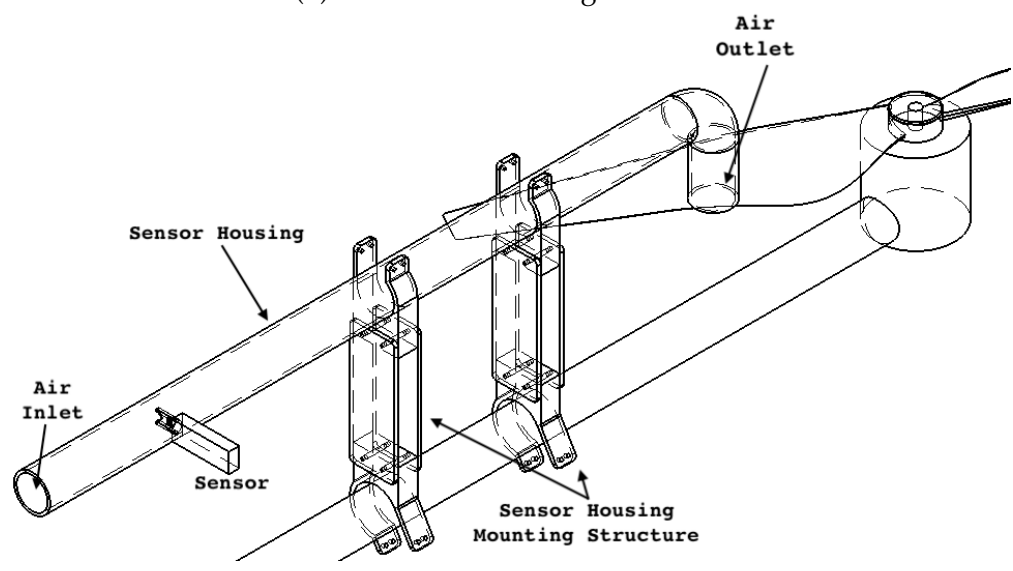


(c) Uwash housing schematic

Figure 4.3: Sensor housing first iteration Schematic

Figure 4.4: Sensor housing configurations used during solar eclipse Flight

and mixing of air causes error in measurements.

These findings prompted the next design iteration: upwash housing with inlet pointing outside UAS.

## 4.2 Sensor Housing: Second iteration

The sensor housing exploits the pressure deficit created on the top of a spinning multirotor propeller to induce high speed airflows inside itself. The passive-indirect draw of air, by positioning the housing air intake *above* the propeller, creates a laminar flow at the inlet. The sensor housing is designed by following the fluid dynamics textbook [42] to have recommended angle of expansion/reduction ($20° - 45°$) and radius of curvature ($r/D > 0.2$) for the air inlet which ensures

(a) Schematic of the sensor housing.

(b) Building blocks of the housing.
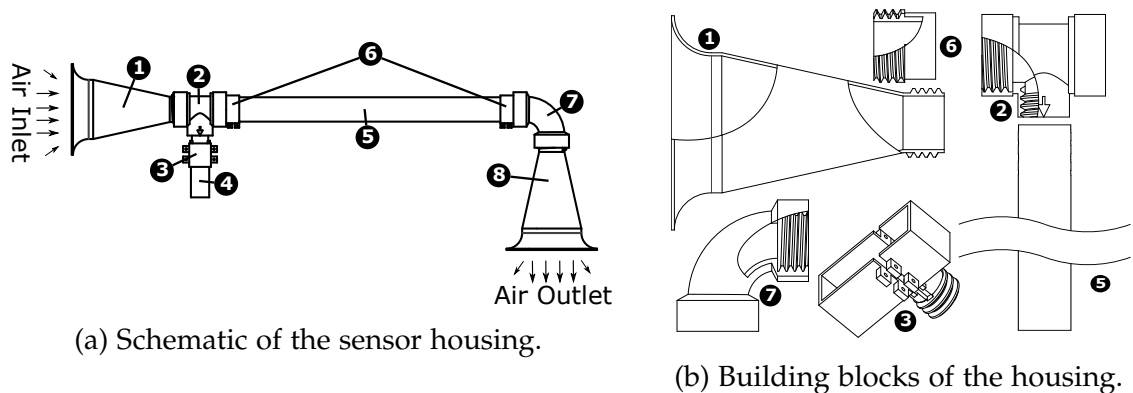
Figure 4.5: **1** Inlet, **2** Housing-Sensor Holder Coupler, **3** iMet XQ2 Sensor Adapter, **4** iMet XQ2 sensor, **5** Carbon Fiber Tube, **6** Carbon Fiber Tube Adapter, **7** L-bend, and **8** Outlet.

that the housing maintains a high speed flow throughout the housing with a low minor loss of flow. Besides maintaining a consistent aspiration for the sensor, the housing also shields it from incident solar radiation and other heat sources.

The sensor housing, as shown in Figure 4.5a,b, is made from seven components (with an identical inlet and outlet). The individual parts connect using mechanical screw-in threads, which makes it easy to assemble. The primary components of the housing are the inlet, outlet, carbon fiber tube adapter, housing-sensor holder coupler, sensor adapter, L-bend, and carbon-fiber tube.

- **Inlet/Outlet:** The Inlet/Outlet of the sensor housing is designed to have a high cross-sectional area at the end of the inlet/outlet to maximize the airflow rate for a given pressure difference (low pressure on top of the propeller vs, atmospheric pressure outside the UAS body). The reducer-expander strategy (funnel shape) allows the low-speed flow at the intake to flow at a higher speed proportional to the reduction of the cross-sectional area according to the continuity equation, *VolumeFlowRate = Velocity * Area = constant*. The

curved-horn shape of the part creates a smooth transition from a high cross-sectional area at the intake to the narrow cross-section of the carbon-fiber tube, which ensures laminar flow at the inlet of the housing. The radius, $r$, of this curvature and gradient of this curve are chosen to be $\frac{2}{3} * (Tube\ radius)$ (curvature of well rounded inlet $r/D > 0.2$ [42]) to minimize the loss of airflow and to maximize the flow velocity inside the tube. For the housing used in the thesis inlet/outlet transitions from a diameter of 104 mm to 26 mm to match the carbon fiber tube, this reduction in diameter corresponds to a 16× increase in the speed from the inlet through the carbon-fiber tube.

- **Carbon-Fiber Tube Adapter:** This adapter adds on to the standard carbon-fiber tube to make them compatible with the mechanical screw-in threads of the other parts.

- **L-bend:** L-bends transition the flow in a perpendicular direction, allowing the safe extension of the sensor housing outwards parallel to the UAS arm while still using the propeller for air drawing. The L-bend is designed to have smooth bend to reduce the flow loss due to the change of direction.

- **Sensor Holder Adapter:** This adapter is molded to fit on the sensor of interest. Due to mechanical screw-in threads, any sensor with an appropriate sensor adapter will be compatible with the housing. The sensor adapter, as shown in Figure 4.5b, is designed for iMet XQ2. Most of the sensors have strict storage requirements due to moisture affecting the quality of the sensor. Since the adapter is easy to attach to the main housing, it can be plugged-in right before the UAS mission, keeping the sensor safe in storage otherwise. This *adapter*-type design choice allows several different sensor designs to be compatible without modifying the rest of the housing.

- **Housing-Sensor Holder Coupler:** This part provides an attachment point for the sensor adapter to attach into the housing. A sensor plugged into this adapter will be inside the tube aspirated by laminar airflow. Due to the modular design, multiples of this part can be connected in series to have an equal number of sensors taking a reading at the same time from the same sampling airflow.

- **Carbon-fiber tube:** The carbon-fiber tube diameter is critically the most important dimension, as it is the primary determinant of how much airflow is achievable through the tube and consequently drives the dimension of all the other parts. The Hagen–Poiseuille equation [11] dictates that the volume flow rate through a tube is proportional to the power of fourth of its radius which means that for the same pressure difference and length of the tube, reducing the radius by half will reduce the volume flow rate to 1/16th the original. The diameter of the tube also needs to be big enough to allow the sensors to be in the center of the tube with sufficient area around it (such that the ratio of sensor cross-section area to the cross-section area of the tube is small) to promote good airflow. The diameter of the carbon fiber tube used in the thesis is 26 mm.

**Modularity:** All the parts are designed to be modular for ease of replacement and manufacture. The modular design of the housing allows for the addition of multiple sensors to the housing at the same time, while the sensor adapter allows for the replacement of any sensor.

**Ease of production:** The parts are designed to be modular, easily 3-D printed. All the parts except the carbon-fiber tubes are designed to be 3-D printed to reduce the cost of manufacturing and to make them readily reproducible and replaceable in

the lab. Three-dimensional printing imposes additional constraints on the design; for example, Fused Deposition Modeling (FDM) 3-D printers do not provide the same level of strength in the vertical axis of the part and usually have difficulty in printing slanted overhangs beyond 45 ° angle. All the pieces are meticulously designed to satisfy these requirements, resulting in strong, lightweight, and reliable parts.

## 4.3   Sensor Housing: Third Iteration

While the second iteration of housing performed well in terms of measurement reliability, it tends to add additional disturbance to the UAS control system when passing through the turbulent region of the atmosphere. This turbulence is the result of the extension of the housing and support structure outside the UAS body. The airflow inside the second iteration of housing was very high and largely consistent as shown in Chapter 6. However, it had a minor dependency to atmospheric wind corresponding to the inlet pointing against or toward the wind.

The third iteration of housing is designed to alleviate/ improve upon these challenges mentioned above. It is focused on the optimization of the design to provide better integration with UAS with less support structure. The sensor housing is similar to the second iteration in the working principle, and the following improvements are made in this iteration:

- **Dual Outlet:** Housing is modified to have two outlets such that it can be mounted symmetrically on the arm closer to the body of the UAS as shown in the schematic in Figure 4.7.

- **Downward Facing Inlet:** A downward facing inlet is used to decrease the dependency of atmospheric wind speed on the airflow speed inside the

Figure 4.6: Third iteration of sensor housing.

housing. The inlet also provides additional protection from precipitation and flying through clouds.

- **Reduction in Support Structure:** Symmetric design of the housing allows it to be mounted on the arm without the use of heavy support structure. However, the housing requires inverted propeller configuration as shown in Figure 4.6 to be mounted on top of the arm while avoiding interference with the propeller.
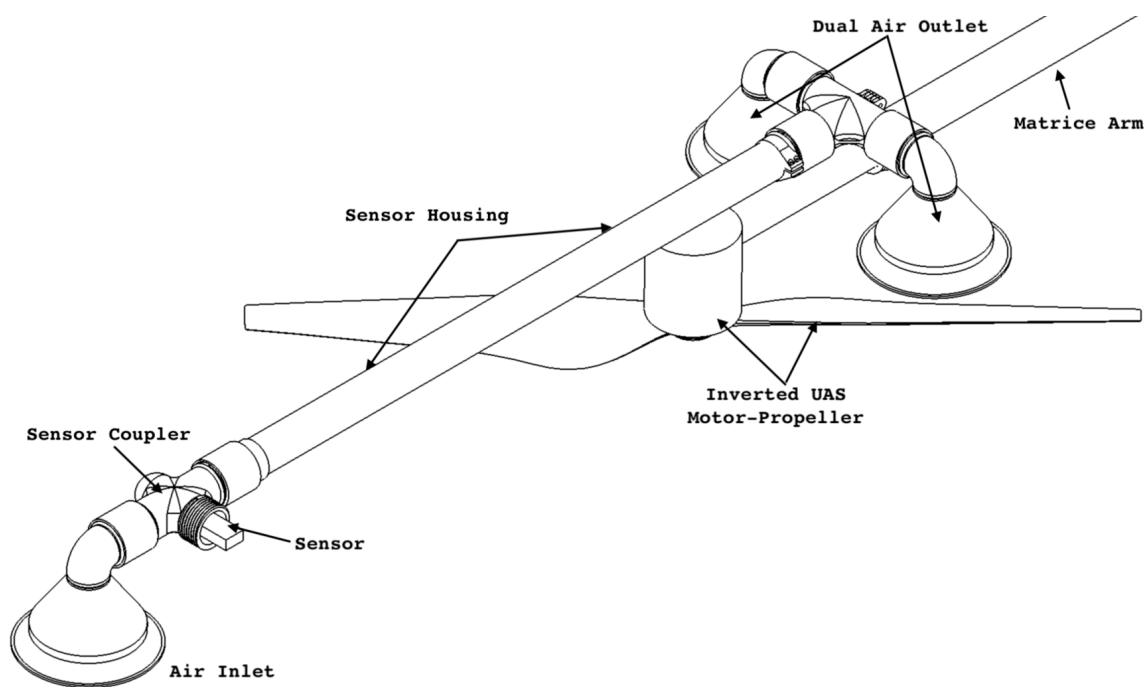
Figure 4.7: Schematic of the third iteration of sensor housing assembly

## Chapter 5

## Materials and Methods

This chapter describes the bench testing in Section 5.1, experimental methods of CLOUDMAP'2017 field campaigns in Section 5.2, and the experimental methods to validate the effectiveness of the second iteration of sensor housing during LAPSE-RATE'2018 in Section 5.3.

Sensor mounting configurations for three flight campaigns are described in Section 3.4. Flight campaigns are discussed in details in Appendix A.3, and summary of the University of Nebraska-Lincoln flight campaigns is captured in Table 5.1.

### 5.1 Bench Testing : Sensor Response Time Comparison

Identifying sensor characteristics allows correction of measured data for system response time. Comparing sensors' performance is also critical to establish reliability of the measurement. It is also important to have sensors with similar specifications when we compare different sensor placement configurations in later experiments with non-identical sensors.

Sensor housing response should be tested as flown [29]. However, to enable the use of freezer as adiabatic chamber, the bench tests are conducted with a

Table 5.1: Summary of the three flight campaigns

|  | Oklahoma'2017 | Nebraska'2017 | Colorado'2018 |
|---|---|---|---|
|  | CLOUDMAP yearly flight campaign | Total solar eclipse flight campaign | LAPSE-RATE flight week by ISARRA |
| Duration | 5 day | 1 day | 6 day |
| Multirotors | 1 Matrice 600 Pro | 1 Matrice 600 Pro | 2 Matrice 600 Pro |
| Housing Configurations (see Table 3.2) | 1, 5 and 6 | 1 and 5 | 7 |
| No. of flights | > 20 | 13 | 170 |
| Total flight duration | — | 215 minutes | 1302 minutes |
| Sensors Used | iMet XQ1 | iMet XQ1 | iMet XQ1, XQ2, nimbus-pth |

bare-minimum housing setup with a smaller footprint( an inlet, outlet, and sensor holder) as shown in Figure 5.1 . An exhaust fan is used with similar airflow speed performance as the housing over the sensor for aspiration.

The primary design objective of this bench test is to compare the response time of the different sensors that are used for TH measurement inside the housing. The sensor is subjected to a step response with a large temperature swing (approx. $40\,°C$) by keeping the aspirated sensor inside the freezer until it reaches equilibrium and then quickly taking it out in the room temperature. The test is also designed to show the effect of the thermal inertia of the housing system as a whole.

## 5.2 Experimental Methods: CLOUDMAP-Oklahoma'2017, and Nebraska'2017

The experiments conducted in CLOUDMAP field campaign in Oklahoma are designed to evaluate the performance of the first iteration of the housing. Experi-
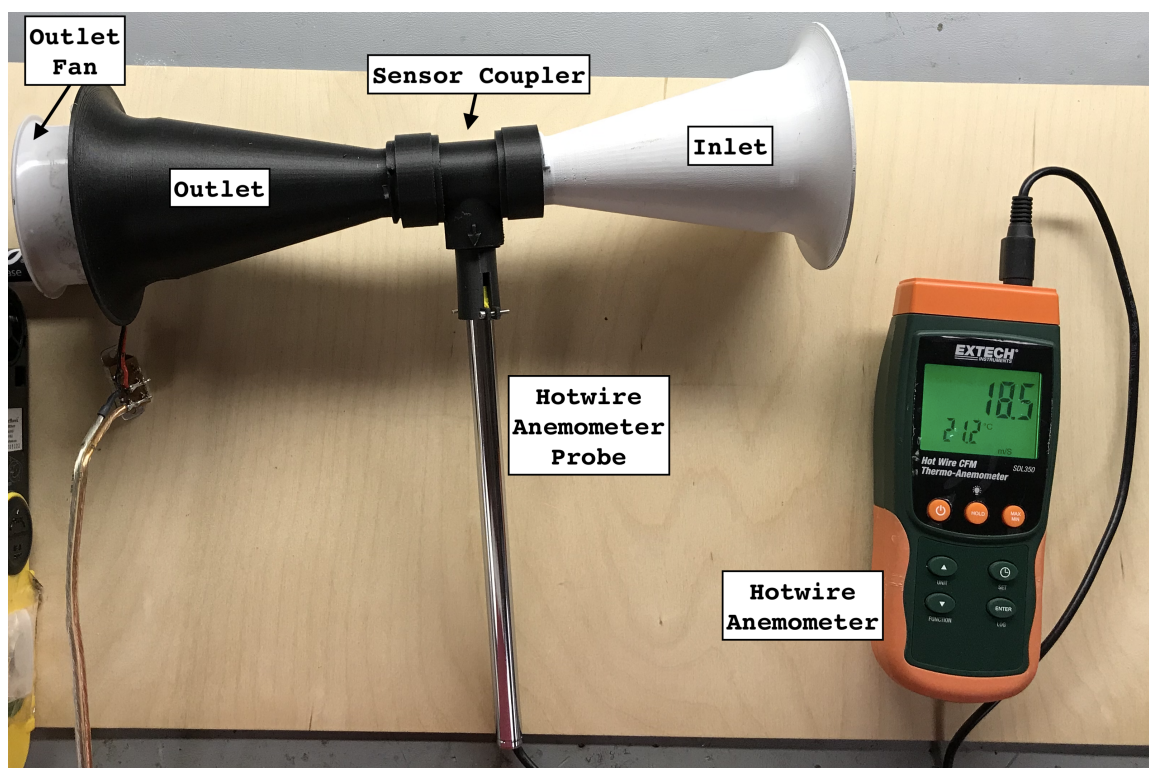
Figure 5.1: Bench testing setup of 'Sensor Response Time Test' showing the airflow inside the housing to be 18.5 m/s using hot-wire anemometer.

ments range from the comparison of sensor response time as flown with ground truth data, the effect of orientation on different sensor placement, comparison of the three sensor placements used in different experiments.

A second campaign using the sensor housing from the first iteration is conducted in Wilber, NE, USA, to observe the temperature changes occurring in the atmosphere during a full solar eclipse. We conducted 13 flights spaced throughout the day, with frequent flights around eclipse time. These flights demonstrate a practical use case of multirotor UAS deployment in remote areas and also prove that the multirotor-housing system is capable of all-day monitoring of atmosphere.

## 5.3  Experimental Methods : LAPSE-RATE'2018

We designed our experiments to verify that the housing meets the design require-
ments (Chapter 3) and is capable of producing accurate and consistent measure-
ments with the third iteration of the housing. The experimental measurements
also evaluate the effect of different horizontal and vertical speeds as well as the
orientation of the UAS.

EXP 1  **Airflow Inside the Housing:** During a field test, the airflow speed inside the
housing is measured using a hot-wire anemometer (Extech SDL 350, FLIR
Commercial Systems Inc., Nashua, NH, USA) to establish the consistency
of the flow speed and its directional dependence on the ambient wind. We
conduct ten vertical profiles at the same location within 13 minutes with the
successive $36°$ changes in the orientation of the UAS between each ascent or
descent. An analysis of this data would establish that the housing provides
sufficient aspirations at all times, irrespective of the UAS altitude and relative
orientation of the housing with atmospheric wind.

One of the limitations of this experiment is that the atmospheric wind can
vary in direction during the experiment; however, it is considered to be fixed
in direction and speed considering the short duration of the experiment.
Another limitation is that the propeller speed changes during the flight based
on UASs control input; this fluctuation can also result in fluctuation of airflow
speed inside the housing, which is not considered in this experiment.

EXP 2  **MURC Tower Calibration:** Through the LAPSE-RATE field campaign, we
compare our data against the ground-truth data obtained from the MURC
tower, as shown in Figure 5.2. We perform these experiments to investigate

(1) how accurately a sensor inside the housing captures the measurements in-flight when compared with the ground-truth and (2) whether the precision of the sensor is affected by external heat/radiation, resulting in measurement drifts.

We use a similar flight pattern for both UASs (M600P1 and M600P2) by having the UAS climb up to the MURC tower altitude of 15.2 m and hover for 10 min. We also assume that the atmospheric parameters do not change within the horizontal distance of MURC and the UAS, as shown in Figure 5.2b.

Limitations of this experiment are that the sensors used in MURC do not have the same specifications as the ones in UAS. The filtered response of MURC sensors compared with raw data of UAS sensors might appear to be less accurate/precise when looking at the numeric comparison. As such, numeric results should be accompanied by the time-series comparison to reveal the true nature of sensor precision or sensitivity.

EXP 3 **Comparison of Flights at Different Vertical Speeds:** Due to the dynamic response characteristic and sensor response time, measurements made during ascent and descent at the same AGL altitude are expected to have a difference. This difference is proportional to the sensor response time and aspiration airspeed [19]. Since the housing is expected to maintain sufficient airspeed over the sensors at all times, the impact of the UAS vertical speed on the sensor response time should be negligible. Some recirculation of air from underneath the propeller is expected during hover or slow ascent/descent speeds. If the housing samples from the recirculated air, it will result in a measurement error or a reduction of feature details in the observation. As such, we hypothesize that the housing would allow missions with faster

ascending speeds, reducing the flight duration for similar altitude profiles. We test this hypothesis over ten flights with different ascent and descent speeds and compare the absolute error between the ascent and descent measurements. The UAS used in our experiments is limited to a maximum vertical speed of $5\,\text{m/s}$ during ascent and $3\,\text{m/s}$ during descent.

The limitations for this experiment is that we assume ascent-descent difference is only affected by UAS speed. However, microscopic turbulence due to convective mixing in the atmosphere can also affect this reading. Also, measured data may appear smooth when the UAS travels at a faster speed and may not detect the micro-scale changes due to sensor response lag.

EXP 4 **Inversion Layer Tests:** We conduct the inversion layer tests to investigate whether the sensor is exposed to mixed and turbulent airflow of the UAS. Well-mixed air will not exhibit an inversion layer. If the UAS flies through an inversion layer and the TH sensor samples from the UAS mixed air, it will not be able to detect it. Hence, if a sensor inside the housing can detect an inversion at the true altitude, it will validate that the housing is not sampling from mixed air. Additionally, if there is an issue with aspiration, this will also make it harder to identify inversion. We perform the flights through an inversion layer (ground truth established using balloon radiosondes) at different ascent and descent speeds. We also conduct horizontal transects (at an altitude of $50\,\text{m}$) to investigate if the sensor readings are consistent when the sensor is in the wake of the UAS.

- **Vertical Profiles:** We perform six flights at different ascent and descent speeds. We place the sensors in upstream (the sensor is mounted on end directly facing the wind) of the UAS M600P1 and downstream

(the sensor is mounted on end facing away from the wind) of the UAS M600P2. Identification of the inversion layer with these profiles establishes whether the housing is sampling from the UAS's disturbed airflow, the effect of the orientation of the UAS relative to the wind, and the presence of aspiration issues. Flights are also performed at different speeds to establish the effect on the sensor measurements.

We assume the mean TH profile stays same when comparing ascent/descent. The effect of air-mixing on TH due to UAS propeller movements is also assumed to be negligible.

- **Horizontal Profiles:** These experiments investigate the effect of ambient wind and the UAS's relative orientation on the sensor measurements, especially for horizontal profiles. Our experiments were conducted such that the sensor is exposed either upstream (sensor on the leading front of the UAS) or downstream (sensor mounted on the trailing end of the UAS motion).

  It is assumed that in the nocturnal boundary layer and without the presence of convective mixing, TH profile at a fixed altitude will be iso-thermal for the case of small horizontal movements.

- **Comparison with Radiosonde Balloon:** We use two radiosonde balloons launched one hour apart as our source of ground truth for the inversion profiles. The release of the first balloon coincides with the first vertical profile, while the second balloon is launched at the start of the horizontal profiles. We use the data from the radiosonde for comparison against the ascent data recorded by the UAS to assess how well it captures an inversion.

(a) Ten minutes of hover flight calibration of the UASs (M600P1 and M600P2) with MURC (Mobile UAS Research Collaboratory).
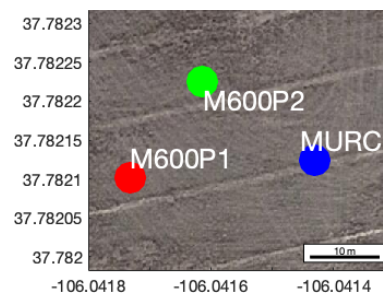


(b) Horizontal placement of UAS and MURC as shown with latitude in y-axis and longitude in x-axis. Image Courtesy of Google Map

Figure 5.2: MURC tower calibration.

## Chapter 6

## Results

This chapter describes the result from the bench tests in Section 6.1, CFD simulation results are discussed in Section 6.2, key results from CLOUDMAP'2017 field campaigns are described in Section 6.3, and results from LAPSE-RATE'2018 field campaigns are detailed in Section 6.4.

## 6.1 Bench Test: Sensor Response Time Comparison

Sensor response time test as shown in Figure 6.1 shows that the response from both the commercially available sensor iMet-XQ2 and lab-built sensor nimbus-pth performs very similar. As such, response time of nimbus-pth is same as iMet-XQ2 manufacturer's specifications of 1 s. However, the overall response time for both sensors appears slightly sluggish ($\approx$ 0.5 *seconds* slower). The thermal mass of sensor housing has an inherent response delay and could contribute to the slow responses. However, in real life deployment of the housing, such a high-temperature swing in a very short period of time is not expected, and as such, the sensor housing might not impact the overall response time of the system. Further experiments can be done to verify the response time constant of the housing as flown given the availability of large adiabatic chambers.
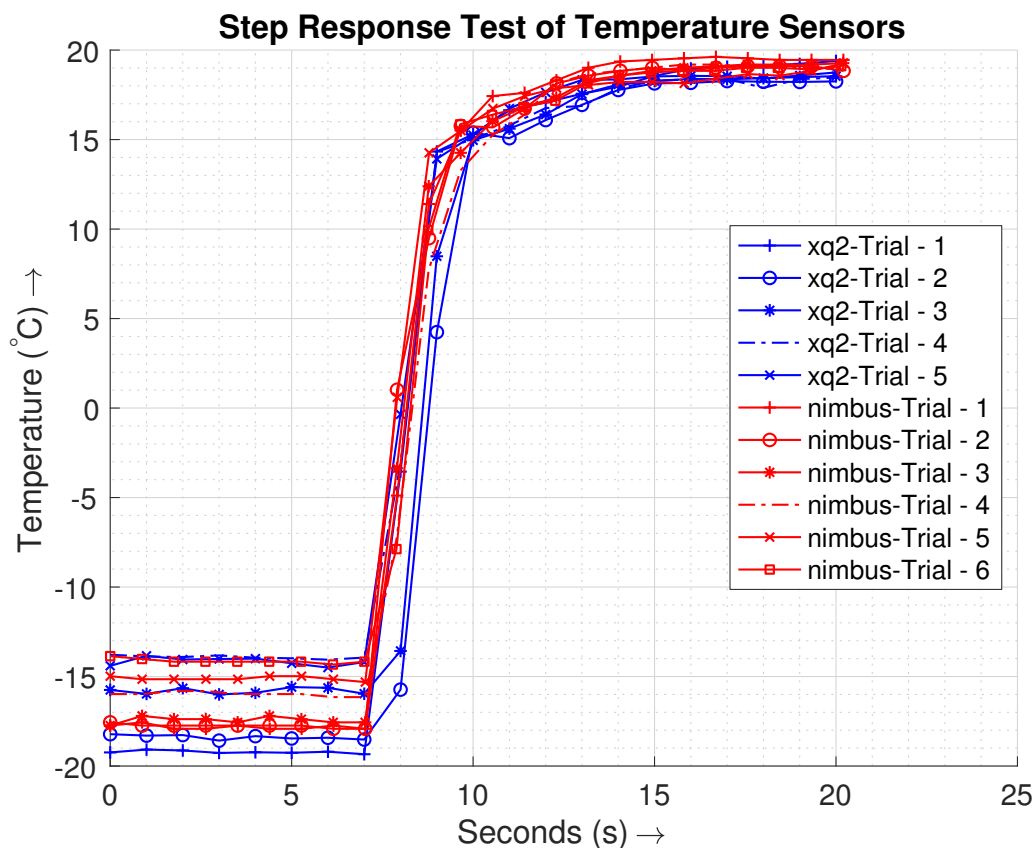
Figure 6.1: Temperature step response test for iMet-XQ2 and `nimbus-pth` sensors. The sensor is allowed to sit inside the freezer until reach steady equilibrium temperature and then quickly taken outside with inlet pointing upward to allow room temperature air to pass through the setup.

## 6.2 Air Flow Inside the Housing : CFD Simulation

Airflow inside the housing is tested through SolidWorks CFD simulations using similar propeller such as the one used on the UAS. Simulation results presented in Figure 6.2 shows the source of airflow is far removed from the UAS turbulence. The images also show that there is some re-circulation of air inside the housing during hover. The air around UAS body is most turbulent during the descent and hence is required to be sourced from outside UAS body. Ascent/descent speed of the UAS is set to be $2\,\text{m/s}$. In the simulation, a speed of $\approx 4\,\text{m/s}$ of air flow

is achieved when the propeller speed is set to 6000 RPM (typical UAS propeller speed). However, the airflow inside the second iteration of housing is found to be 12-14 m/s during actual flight. The discrepancy in speed is possibly due to the shape mismatch of the propeller used in the simulation when compared to the actual UAS. Further research with pressure sensor mounted at the inlet and outlet of the physical sensor housing can be used to identify the discrepancies with simulated sensor housing.

## 6.3  Results from CLOUDMAP - Oklahoma and Nebraska'2017 Field Campaign

Due to the sensor response lag, a difference of reading between ascent and descent is expected. Figure 6.3 shows a comparison of ascent and descent for all three sensor configurations in the first iteration of housing.

Direct downwash housing seems to have the lowest error (ascent-descent) among the sensor configurations. However, the noise in data indicates uncertainty in aspiration. Both downwash housing and upwash housing shows signs of insufficient aspiration. Since the downwash housing has high airflow speed inside the housing, the underlying reason could be pulling in mixed air inside the housing. Upwash housing, on the other hand, could be affected by insufficient aspiration during descent as it lies in the wake of UAS.

Figure 6.4 shows the effect of the solar eclipse on the atmospheric boundary layer. During the total eclipse, the temperature near the ground decreases dramatically and causes inversion in the temperature profile. Progression of temperature throughout the day is shown in Figure 6.5.
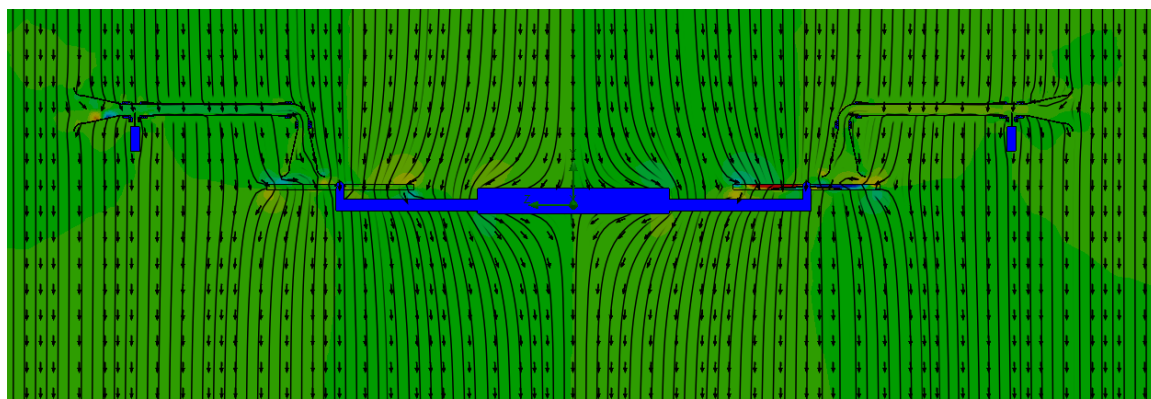
(a) Ascent
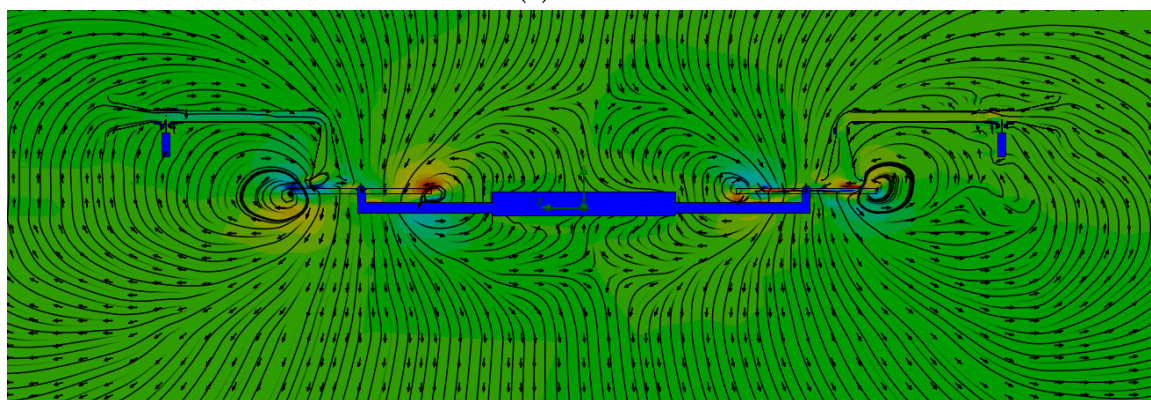


(b) Hover
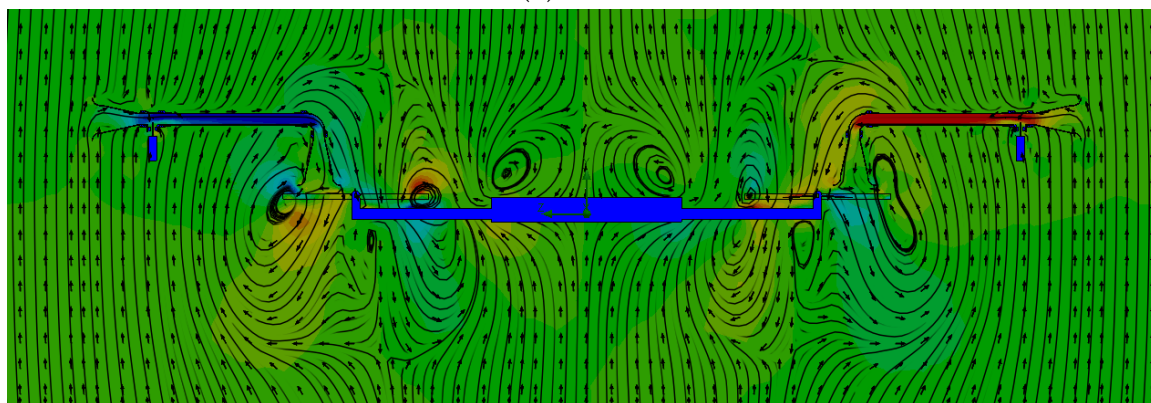


(c) Descent

Figure 6.2: CFD Simulation of a simplified UAS with the sensor housing. Ascent/descent speed is 2m/s. Colors in the image indicate airspeed with respect to horizontal axis with blue and red being the lowest speed and highest speed in positive horizontal axis.
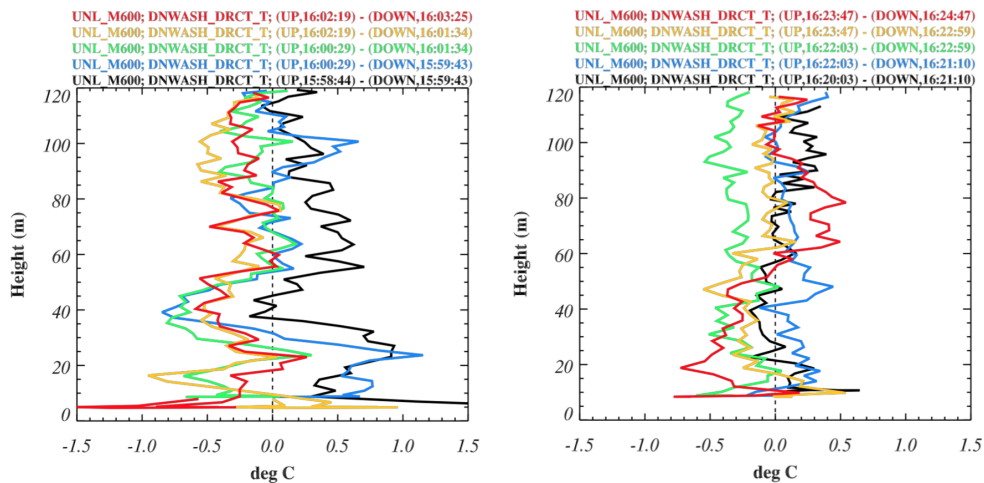
(a) Direct downwash housing
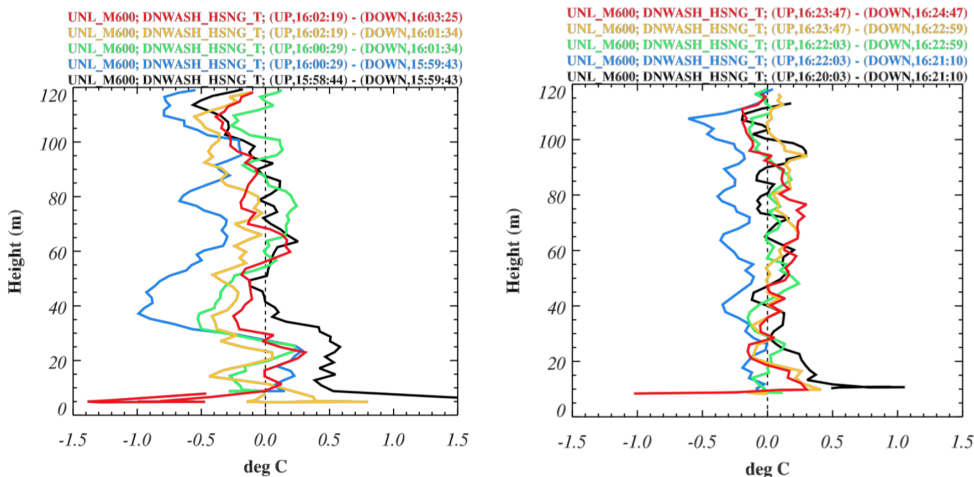


(b) Downwash housing
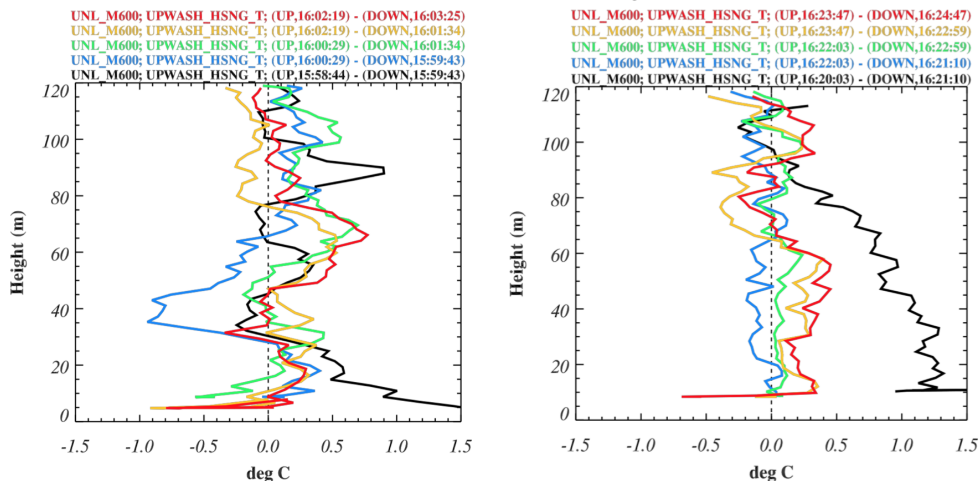


(c) Upwash housing

Figure 6.3: Comparison of ascent (up) and descent (down) by evaluating the difference at similar altitude. Results from Houston *et al.* [20].
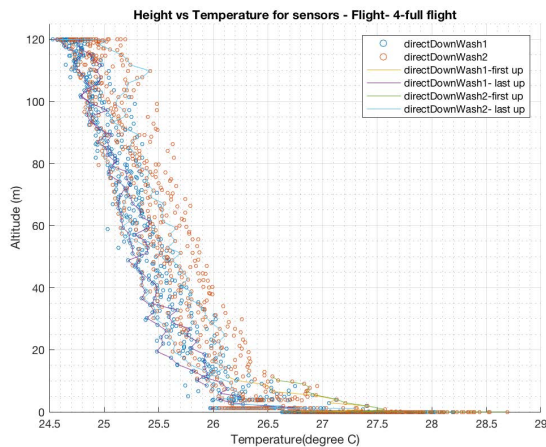
(a) Flight before total eclipse
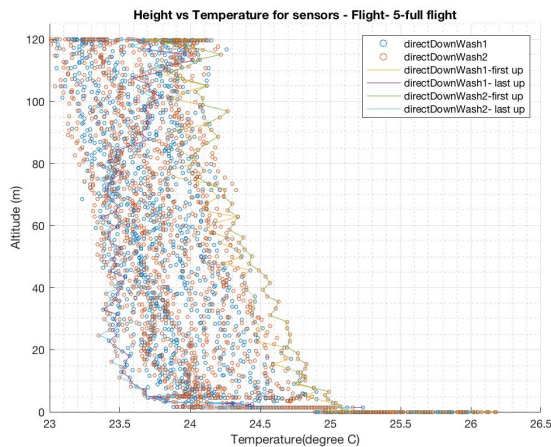


(b) Flight during total solar eclipse
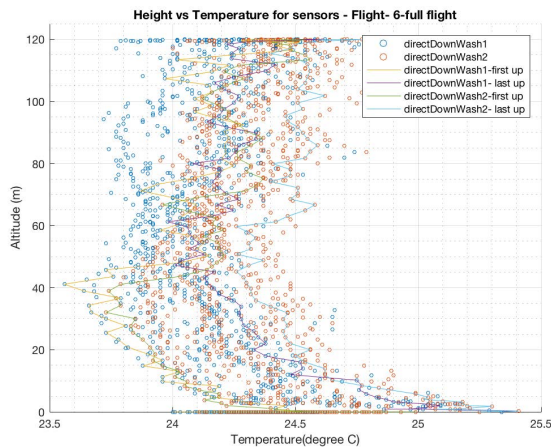


(c) Flight after total eclipse

Figure 6.4: Temperature vs Altitude effect of solar eclipse where solar eclipse causes inversion near surface.
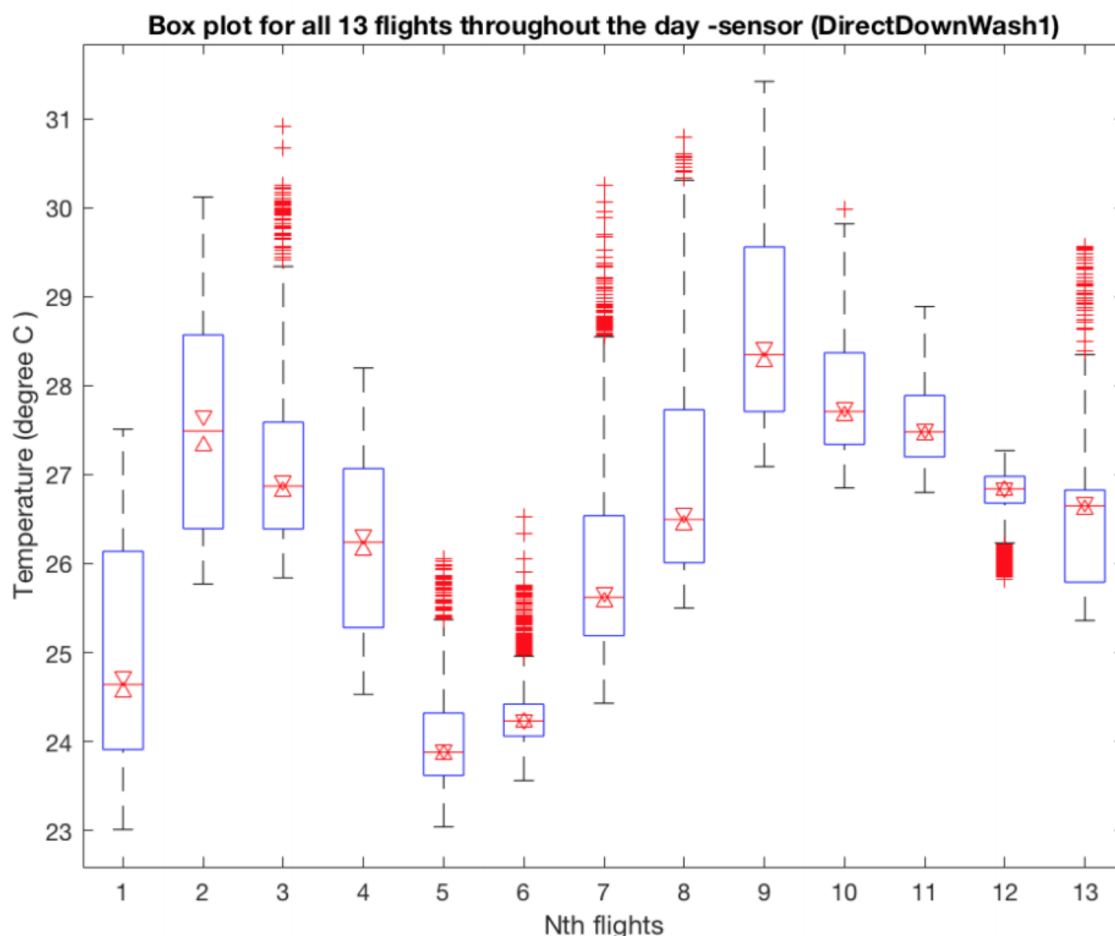
Figure 6.5: Temperature box plot throughout the day. Total solar eclipse happened during flight 5.

## 6.4 Results from LAPSE-RATE Field Campaign (Housing Version no. 2)

The results are presented in sections same as that in the *Experimental Methods* (Section 5.3). We note that, for all the following analysis, the data from MURC and radiosonde are filtered by the manufacturers' proprietary algorithms. However, the data from the UAS is not filtered or corrected for sensor response lag. The thesis focuses on capturing the impact of sensor housing on the observations/data collection. Filtering could wash out the difference in post-processing depending

upon the details available in the observation. If the raw data does not capture the details accurately, post-process filtering would be impacted as well.

Assuming the ascent and descent profiles are identical at the same location within a reasonably short time-frame, they would appear symmetric/mirrored around the corrected profile if the sensor data is not corrected for sensor response lag. We do not perform such corrections for the data presented in this thesis; standard post-processing can take them into account [29].

### 6.4.1 (EXP 1) Airflow inside the Housing

This subsection describes the results from experiments described in EXP 1 of Section 5.3. Figure 6.6 shows the actual airflow speed inside the housing during flights, as measured by an anemometer. The box plots show the distribution of flow speed for ten flights with different relative orientations of atmospheric wind over altitudes ranging from 5 m to 120 m above ground. As seen from the plots, the mean flow speed inside the housing is 12.45 m/s (with a variance of 1.25 m/s), which is roughly $2.5\times$ the required aspiration for the iMet sensors used in the thesis.

Although the housing is designed to have smooth flow at the inlet, high aspiration airspeed also indicates presence of turbulent airflow inside the small diameter tube (Reynolds number of $\cong 20604$).

### 6.4.2 (EXP 2) MURC Tower Calibration

This subsection describes the results from experiments described in EXP 2 of Section 5.3. Figure 6.7 shows a time-series of the temperature (T), and humidity (RH) sensor readings for a 10 min hover along with the MURC tower readings. Since the sampling rate and the timestamp of data-recording are not the same
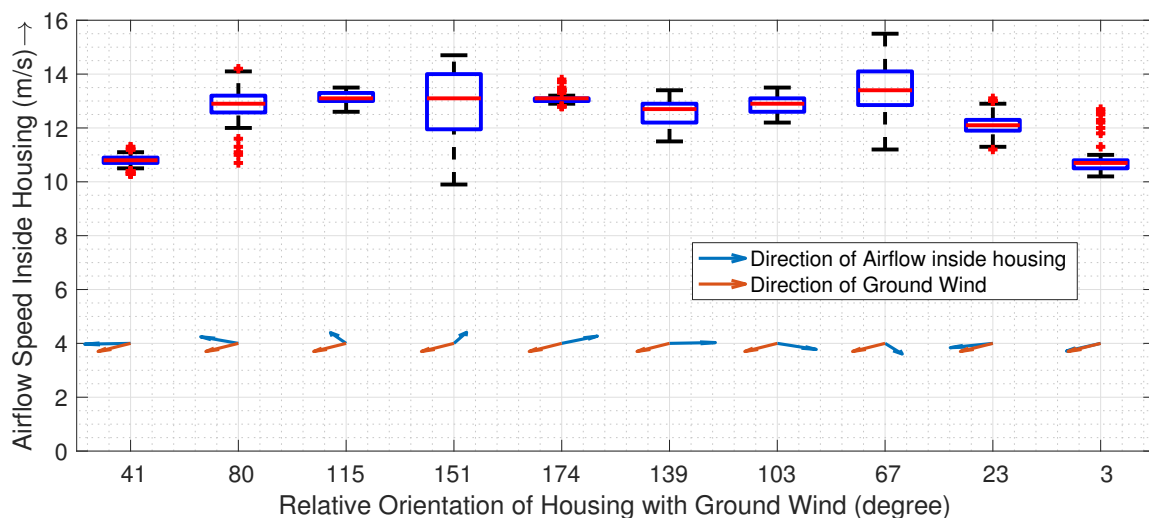
Figure 6.6: The plot shows sensitivity in the airflow speed inside the housing in the presence of wind for ten consecutive flights at different orientations of the UAS from the north at a ground wind speed of 6 mph from the northeast. The box plot captures the 25th to the 75th percentile of data, while the central red line indicates the median. The black whiskers and the red plus signs indicate the extreme range and outliers respectively.

for all the sensors and MURC, all of the measurements from the UAS have been resampled linearly according to the time-stamp of the MURC data (with the assumption that the MURC and UAS clocks have no relative offset among them).

The time series shows that sensors used on the UAS are more sensitive to changes than those on the MURC and that the resolution of the temperature sensors are $10\times$ of the MURC. A visual inspection also reveals that the sensors show a similar trend with MURC but with an artificial response time offset (MURC lags $\sim$40 s for the temperature sensors and $\sim$9 s for the humidity sensors).

If the time stamp on all the devices are accurate and synced using GPS, this could be a result of spatial variation where the horizontal wind carried a higher temperature air from a different place through these devices at different times. Alternatively, more likely due to the ill-matched time offset for temperature and humidity, the sensor response time of MURC could be higher, causing it to lag,
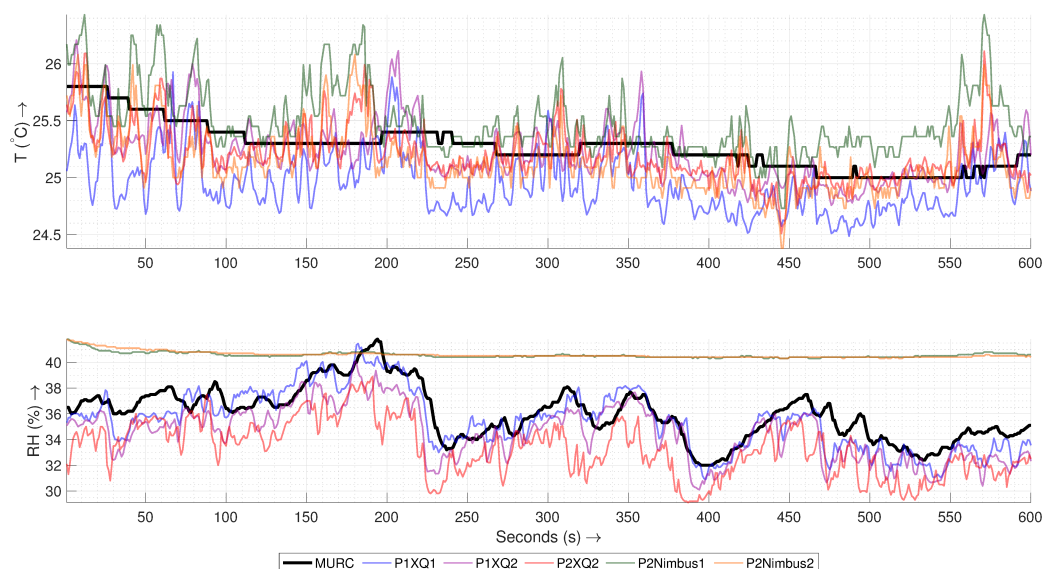
Figure 6.7: The Temperature (T) and Humidity (RH) time series of the MURC tower and other sensor readings for the 10 min of hover of the UAS at the MURC tower altitude (15.2 m): Only the data from MURC is filtered and corrected for sensor response.

especially if it is aspirated by the atmospheric wind with an insufficient speed which may increase the response time. Another reason for the time offset could be the fact that a smoothing algorithm is in place for MURC with large moving average window. Another important thing to note is the humidity sensor response of P2Nimbus1 and P2Nimbus2. These two sensors, if plotted separately, show a similar trend as that of other sensors, but the sensitivity of the sensor appears to be very low and hence appears as a straight line when plotted together with the others. We see this effect throughout all the experiments where the humidity measurements of `nimbus-pth` are usually less sensitive to changes and could be at an offset with standard sensors. The data gathered from these sensors would still provide valid insights, and the effect could be corrected by tuning through the analog-to-digital conversion process for these sensors.

The absolute errors are within the bound of sensor uncertainty, as shown
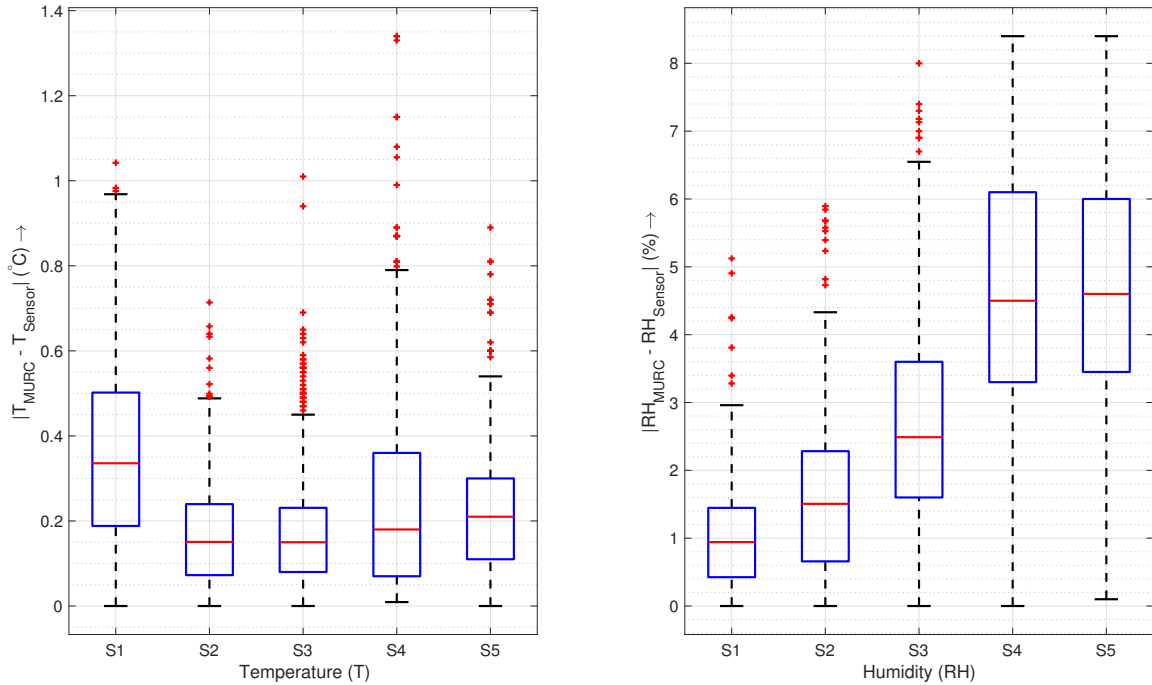
Figure 6.8: A comparison of the sensor readings with the MURC tower: The data presented here summarizes 10 minutes of hover at the MURC tower altitude (15.2 m) as presented in Figure 6.7. (S1—P1XQ1 (housing), S2—P1XQ2 (housing), S3—P2XQ2 (housing), S4—P2Nimbus1 (no housing), and S5—P2Nimbus2 (housing)).

Table 6.1: The key statistics for the MURC calibration error ($MURC - Sensor$).

| Sensor | Temperature (°C) | | | Humidity (%) | | |
|---|---|---|---|---|---|---|
| | Mean | Variance | RMS | Mean | Variance | RMS |
| P1XQ1 | 0.32 | 0.064 | 0.41 | 0.51 | 1.324 | 1.26 |
| P1XQ2 | 0.05 | 0.043 | 0.21 | 1.51 | 1.546 | 1.96 |
| P2XQ2 | 0.07 | 0.048 | 0.23 | 2.70 | 2.266 | 3.09 |
| P2Nimbus1 | −0.22 | 0.075 | 0.35 | −4.56 | 3.915 | 4.97 |
| P2Nimbus2 | 0.13 | 0.059 | 0.28 | −4.58 | 3.870 | 4.99 |

in the box plot in Figure 6.8, for sensors in the housing, whereas the sensor without housing (P2Nimbus1) has a higher range of errors with an increased variation in reading. The primary source of error in both figures is the difference in resolution and the artificial time offset, as discussed above. The key statistics of the measurement errors are presented in Table 6.1.

### 6.4.3 (EXP 3) Comparison of Flights at Different Vertical Speeds

This subsection describes the results from experiments described in EXP 3 of Section 5.3. This section presents the results from different ascent/descent speed combinations to find the ascent/descent speed pair that works best for the housing. Since we do not capture all ten profiles simultaneously and the variability in speed causes unequal data points among profiles, we plot TH against the altitude instead of plotting them as a time-series as we did for the MURC comparison. Figure 6.9 shows the temperature and humidity plotted against the altitude for five different combinations of ascent and descent speeds. Each row of the plot represents a different sensor as identified on the y-axis label, while the legend on the bottom of each column specifies the order in which we performed the flights. The title of each column of the plot represents the ascent and descent speeds. This figure also provides the grounds for comparison of the housed sensor with a non-housed sensor since P1XQ2 and P1Nimbus2 were inside the housing while P1Nimbus1 was mounted under the body of the UAS without housing. Although we performed the actual flight between 0–150 m AGL, both the ascent and descent data were trimmed to be 10–148 m and resampled at each meter of altitude to facilitate a comparison of the ascent vs. descent. The reason for trimming is to avoid a comparison of noisy data at the ground level and also to reduce the artificial inversion effect at the start and end of the flight due to the sensor's dynamic response [19]. In Figure 6.9b, the humidity sensor on P1Nimbus1 and P2Nimbus2 seems to have an offset of ~20% and, similar to the comparison with MURC, appears to be less sensitive to changes in the atmosphere when compared with P1XQ2. Despite the offset and sensitivity, the sensors still provide relevant features for a comparison based on the vertical speed. Due to the dynamic sensor response characteristic

and corresponding time constant, a finite amount of difference is expected when we subtract the temperature profiles of the descent from the ascent ($\Delta T$). This difference is expected to increase with the speed of ascent/descent and to decrease with the aspiration airspeed [19].

As seen in Figure 6.10a, sensors inside the housing are not affected by the vertical speed as much as the sensor without it. The $\Delta T$ on the housed sensor, which is sufficiently aspirated, increases significantly slower compared to the non-housed sensor as vertical speed increases. This increase in error is merely an artifact of the sensor response time constant, which prevents the sensor from *catching up* to larger step changes in temperature. The increase in the ascent/descent speed appears to add additional burden on the "effective" sensor response time, which would cap the maximum vertical velocity of the UAS for an accurate profile. However, the sensor inside the housing can exploit the maximum UAS capability for speed without significantly changing the response time.

Another interesting feature to note is that, when the descent is slower than the ascent, the difference appears to be lower than that of same ascent/descent speed (since a lower speed will produce values closer to the actual value). There is also an interesting trend in the humidity box plots in Figure 6.10b for P1XQ2: The range of absolute error decreases (while the mean error is still under 2%) with the increase in vertical speed. This decrease is the result of sensors not picking up the fine-scale changes in the atmosphere at faster speeds, making the data appear smoothed out. A comparison of the sensors shows an increase in the humidity error (ascent-descent) when the sensor is non-housed, which exacerbate as the vertical speed increases. It should be noted that the humidity sensor response time is dependent on the temperature, as specified in Table 3.2.

(a) Temperature (T)



(b) Humidity (RH)
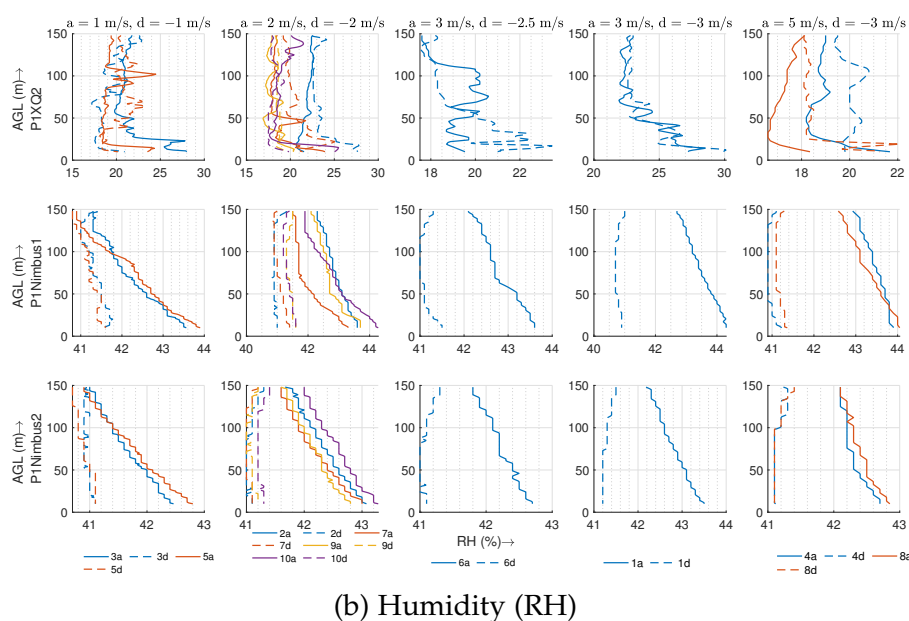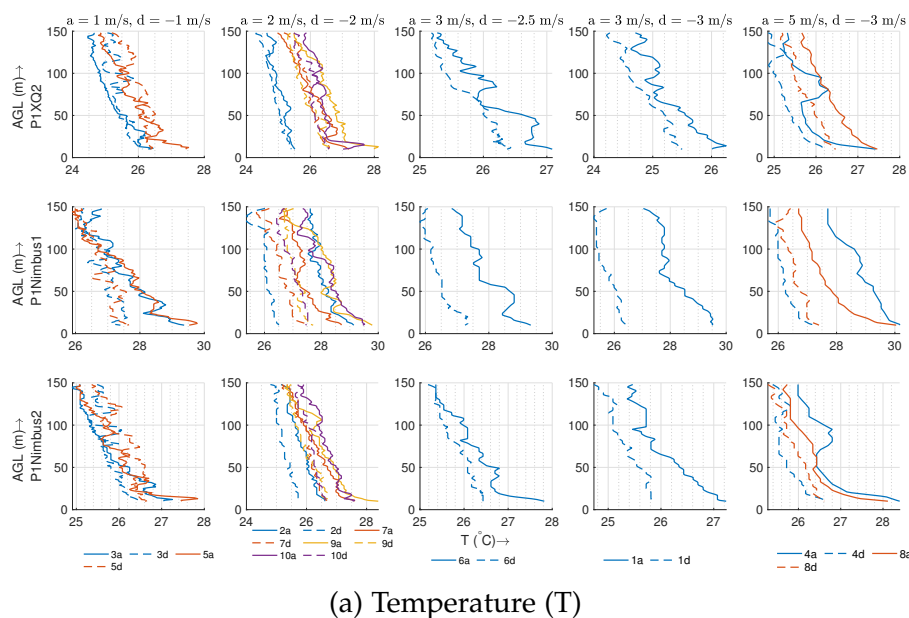
Figure 6.9: The plot shows the ascent (**a**) and descent (**b**) temperatures against the altitude for 10 consecutive flights conducted over a period of 60 min (7/18/2018 7:21 pm UTC–8:20 pm UTC) at different *"a"* and *"d"* speeds mentioned in the title of each subplot. Multiple flights at the same speed are grouped. The colored legend under the plot indicates the order in which the flight was performed. The sky was slightly cloudy with cumulonimbus clouds, and the ground wind was 4–5 m/s from the NW. The data presented in this plot is not filtered or corrected for sensor response characteristics.
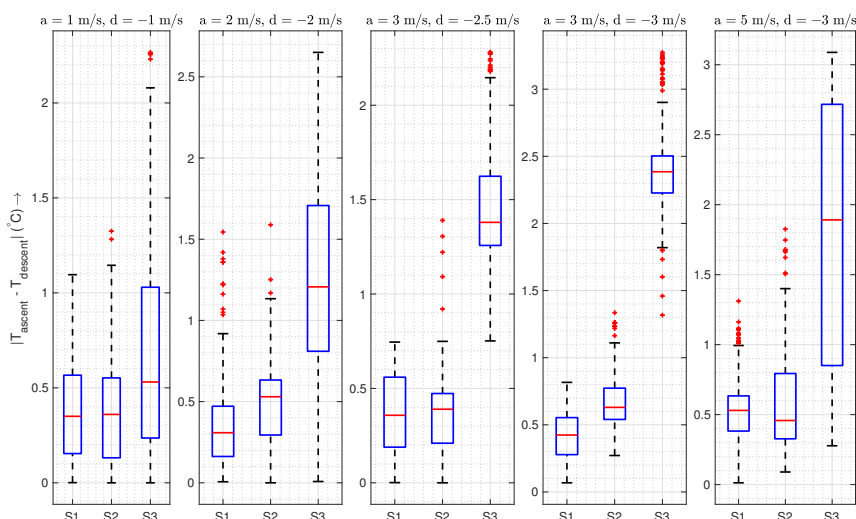
(a) Temperature (T). (S1—P1XQ2 (housing), S2—P1Nimbus2 (housing), and S3—P1Nimbus1 (no housing))
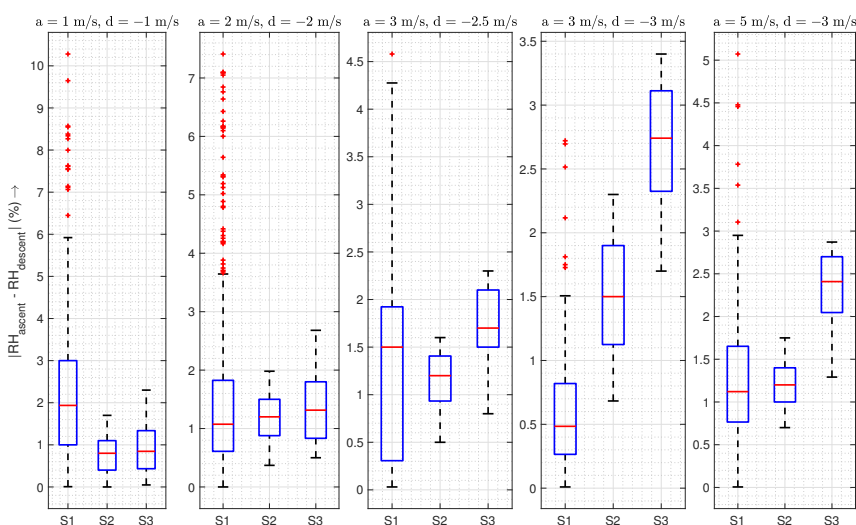


(b) Humidity (RH). (S1—P1XQ2 (housing), S2—P1Nimbus2 (housing), and S3—P1Nimbus1 (no housing))

Figure 6.10: The box plot summarizes Figure 6.9 by showing the absolute (ascent − descent) temperature and humidity differences for 10 consecutive flights conducted over a period of 60 min (7/18/2018 7:21 pm UTC–8:20 pm UTC) at different ascent (**a**) and descent (**b**) speeds mentioned in the title of each subplot. Multiple flights at the same speed are grouped and plotted together. The sky was mostly sunny with cumulonimbus clouds, and the ground wind was 4–5 m/s from the NW.

### 6.4.4　(EXP 4) Inversion Layer Tests

This subsection describes the results from experiments described in EXP 4 of Section 5.3. Figure 6.11 represents vertical inversion layer flights at different speeds of ascent and descent, as indicated in the corresponding plots. The figure also features radiosonde data for the same altitude range that was launched a minute before the first UAS flight and 36 min after the sixth UAS flight. For this experiment, we consider only the sensors inside the housing. We note that the relative humidity data for P1XQ2 had to be discarded due to a glitch causing the sensor to be saturated at 100% before the inversion layer tests and hence is replaced by P1XQ1 relative humidity observations. The relative humidity for radiosonde is calculated from the dew point temperature ($T_d$) and air temperature ($T$) using the linear estimation formula as described in [25] to be $RH \approx 100 - 5 * (T - T_d)$.

The temperature profiles in Figure 6.11a demonstrate the ability to detect the inversion at similar altitudes as that of the radiosonde balloon deployed by NOAA. This confirms that sensor housing is not sampling from a disturbed airflow since it would fail to detect the inversion otherwise. The performance of the sensor upstream (P1XQ2) seems to be better than that of downstream (P2XQ2) as the latter seems slightly warmer, which increases as the profile speed increases. These deviations could mean that, even though air is sourced far from the body, a sensor downstream from the wind could be exposed to waste heat from the UAS that is carried by the atmospheric wind (as discussed in Section 3.2). The effect is more significant during ascent if the ascent speed is significantly higher than the wind speed as the resultant wind vector points more towards the air source of the sensor located downstream. Consequently, in such cases, the descent profile matches more closely with the inversion profile.
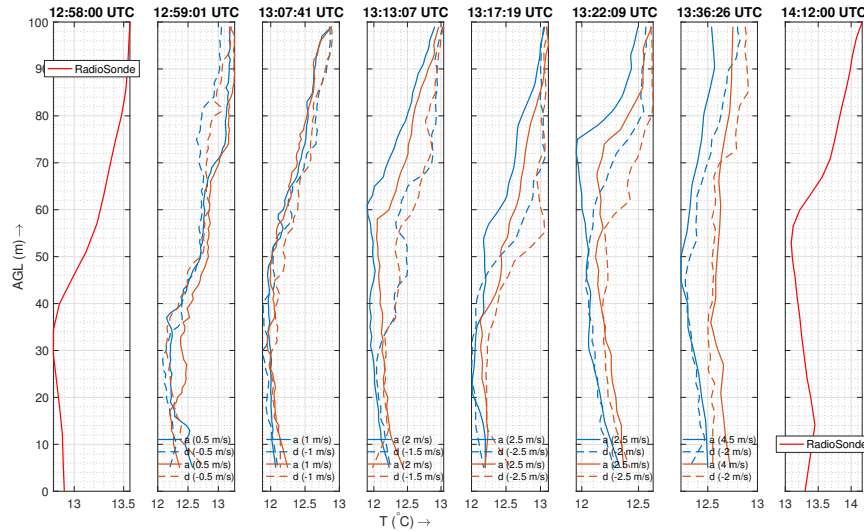
(a) Temperature (T). The blue lines represent P1XQ2, and the orange lines represent P2XQ2.
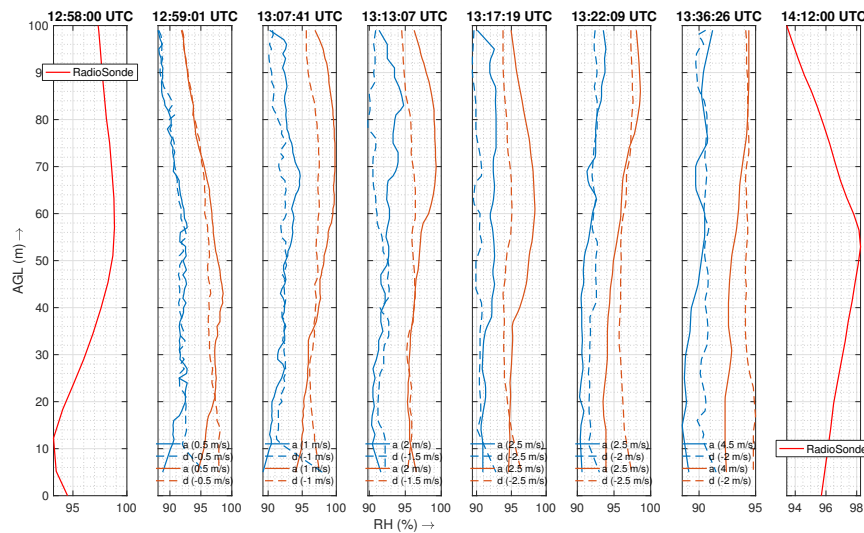


(b) Humidity (RH). The blue lines represent P1XQ1, and the orange lines represent P2XQ2.

Figure 6.11: The plot shows two radiosonde flights (filtered and corrected) and six different flights of the UAS (not filtered/corrected) at different speeds in a inversion layer. The surface wind was 2 m/s from 290–308° relative to north and with a partly cloudy sky. The P1XQ2 sensor is upstream, while the P1XQ1 and P2XQ2 sensors are downstream from the UAS with respect to wind.

The humidity profiles in Figure 6.11b match closely with that of radiosonde at slower vertical speeds. It should be noted that the operating temperature for these missions was low, which decreases the response time of the P2XQ2 humidity sensor. The slow sensor response time combined with the high vertical speed smooths out the data, and the humidity sensor loses the ability to identify a fine-scale inversion.

We performed four consecutive horizontal transects at three different speeds. The direction of each of the four transects along with the direction of air flow inside the housing and surface wind is shown in Figure 6.12. The sensor, P1XQ2, is downstream for transects 1 and 3 and upstream for transects 2 and 4 for UAS 1 (M600P1). The opposite configuration is used for P1XQ1. The sensor on UAS 2 is at a right angle with the direction of movement and hence not subjected to upstream or downstream UAS flow.

Figure 6.13 shows the time series for transects at three different horizontal speeds. For the temperature plots, a sensor that is not subjected to upstream or downstream flow (dashed line, P2XQ2) holds a fairly constant value over both directions of the transect. On the other hand, the sensor subjected to the downstream of UAS (solid line, transects 1 and 3) appears a bit warmer than the sensor placed upstream (solid line, transects 2 and 4). This finding agrees with that of the vertical profiles for the downstream sensors. The effect of sensor warming is more obvious at higher horizontal speeds. The statistics presented in Table 6.2 show an increase in the standard deviation for M600P1 in agreement with the above discussion.

For the relative humidity plots, surprisingly, the sensor subjected to upstream/downstream flow appears more consistent than the sensor not subjected to either stream. Although it is not certain as to what causes this deviation, all the
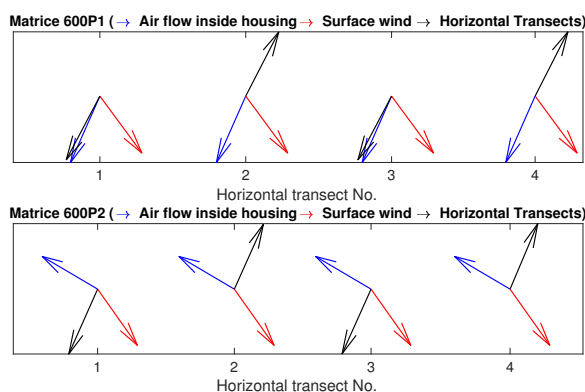
Figure 6.12: The figure shows the air flow, surface wind, and transect direction during each of the four transect flights conducted during each of the three horizontal flights through the inversion layer.

Table 6.2: Statistics for the measurements presented in Figure 6.13.

| UAS Platform | Horizontal Speed | Temperature (°C) | | Humidity (%) | |
|---|---|---|---|---|---|
| | | Mean | Std | Mean | Std |
| | 2 | 12.90 | 0.08 | 91.03 | 1.09 |
| M600 P1 | 5 | 13.44 | 0.06 | 88.71 | 0.98 |
| | 10 | 14.11 | 0.15 | 85.04 | 1.30 |
| | 2 | 13.02 | 0.06 | 93.46 | 1.20 |
| M600 P2 | 5 | 13.59 | 0.05 | 91.59 | 1.41 |
| | 10 | 14.5 | 0.06 | 83.86 | 1.37 |

fluctuations in TH readings are still within the sensor uncertainty.
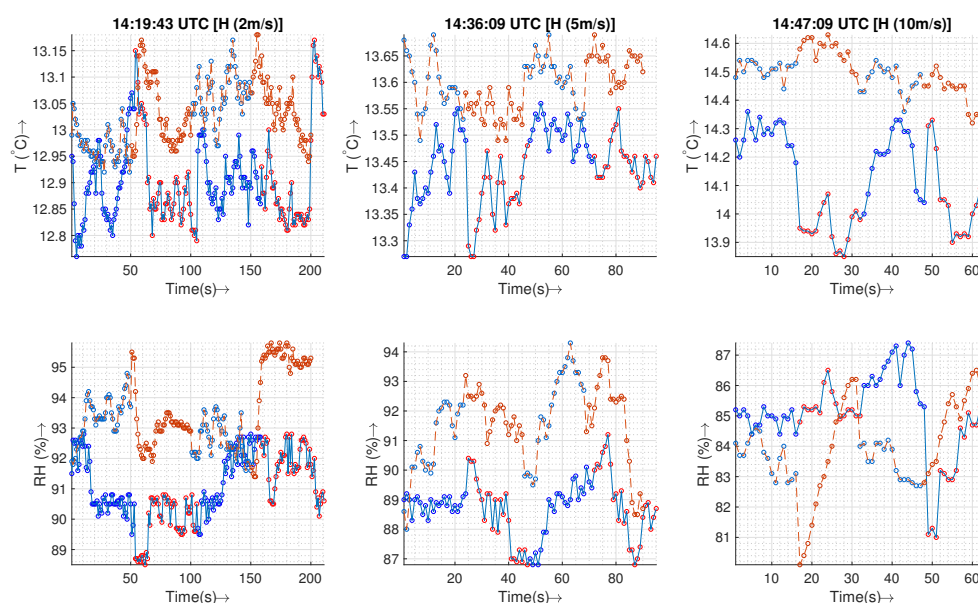
Figure 6.13: The plot shows three different horizontal "transect" flights at different horizontal (H) speeds at 50 m AGL. The surface wind was 2 m/s from 290–308° relative to the north and the sky is partly cloudy. The solid line plots indicate data from M600P1, and the dashed lines indicate data from the M600P2. The blue (M600 P1) and light blue (M600 P2) scatter dots indicate transects 1 and 3, while the red (M600 P1) and orange (M600 P2) are transects 2 and 4. Figure 6.12 shows the direction of air flow inside the housing, the surface wind, and the horizontal transects for each of the transects for both UASs. The data shown here is not filtered/corrected for sensor response characteristics.

**Chapter 7**

**Discussion**

This chapter summarizes the results in Chapter 6 in sections that answers the research questions: is housing better than not having a housing (Section 7.1), what is the effect of UAS orientation (relative to wind and sun) on the housing (Section 7.2), what are effects of housing on UAS (Section 7.3), and what are the ranges of operation successfully tested for the UAS sensor housing system (Section 7.4).

## 7.1  Housing vs. No Housing

A sensor without housing on a UAS has an increased *effective* sensor response time, as seen in the Figure 6.10, which increases with the vertical speed of the UAS. A sensor with higher effective response time is incapable of resolving fine-scale changes and causes an undesirable "smoothing" of the data (Figure 6.9a). According to Figure 6.8, even for stationary purposes such as hovering in one place, a sensor without housing performs worse than a sensor inside the housing.

A sensor housing such as the one presented in this thesis removes a lot of the uncertainty, as it always produces sufficient aspiration (Figure 6.6), is capable of operating at higher vertical and horizontal speeds (Figures 6.10 and 6.13), and

can detect inversion with a comparable performance as a radiosonde balloon (Figure 6.11).

Another significant advantage of housing is its ability to reduce uncertainty in the descent data. Sensors located inside the housing demonstrate similar descent and ascent profiles in both well-mixed air (Figure 6.9) and through an inversion layer (Figure 6.11). These conclusions for the temperature and humidity sensors hold true even when comparing sensors that have similar specifications (such as P1Nimbus1 and P1Nimbus2). The observable difference between the ascent/descent for sensors inside the housing seen in all the plots is a result of dynamic sensor response characteristics and could potentially be corrected if the sensor characteristics are known. To the best of the authors' knowledge, to date, no other housing for multirotors has demonstrated the capability of measuring useful data in both ascent and descent.

## 7.2 Effect of UAS Orientation on the Housing

*UAS Orientation Relative to Atmospheric Wind:* The speed of the aspirating airflow inside the housing varies very little with the orientation of the UAS (Figure 6.6). At a lower speed of operation, a sensor housing downstream or upstream measures values unaffected by the UAS, while slight deviations could be seen when the sensor is located downstream from the UAS at a higher horizontal speed of operation (Figure 6.13). A similar effect could be observed when the sensor is downstream and the ascent speed of UAS is significantly higher than the horizontal wind speed: The ascent appears slightly warmer, which could be contributed by the waste heat of the UAS (Figure 6.11).

It should be noted that, in both cases, the increase is not significant and is

within the uncertainty bounds of the sensors. However, further experiments would be required to establish the effect of the waste heat on the measurements. This could also indicate that the inlet of the sensor housing should be placed even higher to avoid the warmer flow. Alternatively, a wind sensor can be used to reorient the UAS when the desired speed of operations is higher.

*UAS Orientation Relative to Sun:* The primary difference between cloudy and sunny condition will be the incident angle and intensity of solar radiation in the housing. Sensor probes are placed inside the housing, which protects it from incident solar radiation. The housing is made with very thin carbon-fiber material with a very low thermal mass; additionally, all parts are painted with reflective white paint, and solar reflective tape has been used on the carbon fiber tube. With the high aspirating air flow, highly reflective surface, and low thermal mass, the sensor housing is capable of reliable measurements in both cloudy and sunny conditions in any UAS orientation relative to the sun.

## 7.3   Effect of Housing on the UAS

The UAS used in this thesis is capable of a maximum $5\,\text{m/s}$ in ascent, $3\,\text{m/s}$ in descent, and $10\,\text{m/s}$ in the horizontal direction when used in automatic missions. A stricter limit on the descent is because, as the UAS descends into the turbulent downwash, it may start oscillating uncontrollably [12], resulting in a loss of control or crash. Due to the nature of the housing presented here, it extends out $0.7\,\text{m}$ (2.6 times the propeller radius) away from the center of rotor. This requires a second housing to be mounted on the opposite side as well to balance the center of gravity. This comes at the cost of the decreased sensitivity of the UAS in the roll/pitch axis (mounting axis). Traditionally, this sensitivity could be improved by tuning the

flight control parameters. However, that approach is not explored in this thesis to keep the sensor housing generic to commercially available UASs.

Although the structure is quite large, it is very lightweight. There was no loss of control during the 21.7 h of flight time recorded in 170 flights by two vehicles during the LAPSE-RATE campaign. However, for some of the flights, when the vehicle went through turbulent regions of the atmosphere, there was noticeable wobbling in the roll axis (the mounting axis), lasting up to 30 s. Although rare (8 out of 170 flights), the effect would appear more on the descent than on the ascent as the UAS descent on the turbulent airfield created by its propeller. The onset of this oscillation can be detected early on using an onboard computer, as described by Reference [7] and can be countered by slowing down the multirotor speed when passing through turbulent regions of the atmosphere.

Considering these limitations of the UAS, even though the housing is proven to be capable of operating at higher speeds (as seen in the results and the preceding discussion), a near-optimal range of operation would be 0.5–3 m/s for the ascent, 0.5–2 m/s for the descent, and 0.5–5 m/s for the horizontal transect.

## 7.4   UAS Ranges of Operation

Typical ABL profiles are up to 2 km, and the Federal Aviation Administration (FAA, USA) certification of authorization for LAPSE-RATE was valid for up to a 1 km flight. However, software restrictions on the autopilot of UASs limited our profiles to 500 m AGL. The sensor housing is capable of reliable measurements at various temperature/altitude ranges. Data has been collected in different ranges of temperature in various weather conditions and times of the day. To demonstrate the altitude and temperature range capability, additional data collected during the
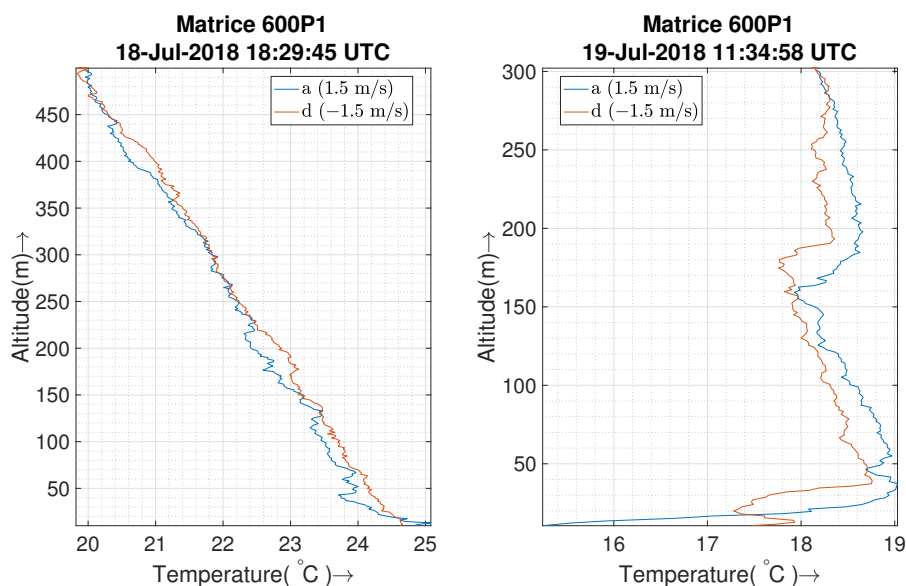
Figure 7.1: The first subplot shows unfiltered temperature data collected from 10 m–500 m of a well-mixed atmosphere at noon with a ground wind of 1.6 m/s with a 5 m/s gust.

LAPSE-RATE campaign is presented in Figure 7.1. The first subplot in Figure 7.1 shows a temperature profile up to 500 m with a temperature difference of $\sim$5 °C between 10–500 meter altitudes at noon when the atmosphere is well-mixed; the second subplot shows inversion detection for a flight up to 300 m before sunrise. Also, the data presented in the Results section such as Figures 6.9 and 6.11 has a 15 °C difference in the operating temperature.

# Chapter 8

# Conclusions and Future Work

In this thesis, we have presented the design and evaluation of a novel sensor housing that allows multirotors to host atmospheric sensors over various profiling missions reliably. The sensor housing features:

- Consistent airflow ($12.5\pm 1.11\,\mathrm{m\,s^{-1}}$) to facilitate fast and precise sensor response time.

- Low standard deviation of measurement ($0.06\,^{\circ}\mathrm{C}$ and $1.2\,\%$ RH) during horizontal transect in iso-thermal layer.

- Low thermal mass and better radiation shielding to reduce radiation error and sensor housing response time constant.

- Provides reliably consistent measurement in both UAS ascent and descent.

- Samples air from a source far removed from UAS turbulence and undesired mixing.

- Is independent of orientation about wind or sun.

- Protects the sensor from artificial heat sources and prevents artificial wet-bulbing.

- Foldable, modular design for fast field deployment and easy replacement.

- Compatible with other sensors with aspiration requirements similar to TH sensors.

We evaluated the nature of the airflow and empirically showed the effectiveness of the housing in maintaining a strong airflow ($\geq 10\,\mathrm{m/s}$) invariant to ambient wind. Numerous field tests conducted at three flight campaigns: CLOUDMAP-Oklhoma'2017, CLOUDMAP-Nebraska'2017, and LAPSE-RATE'2018 flight week which demonstrated the ability of the housing design to precisely capture variations in atmospheric observations, while providing reliable sensor performance during high-speed ascent *and* descent.

The findings in this thesis are also supported by the multirotor/fixed wing UAS platform TH data comparisons of Barbieri *et al.* [3]. The sensor housing described in this thesis used in University of Nebraska-Lincoln multirotors resulted in most accurate and precise readings.

## Future Work

*Sensor Housing Future Improvements:* The sensor housing, as proposed, shows the ability to maintain a sufficiently high aspiration at all times. However, some variability in the speed of aspiration still exists as a function of varying rotor speeds (and possibly ambient wind). If a sensor's response time is highly sensitive to the variation in airspeed, active control of the airspeed might be required. Alternatively, design changes could be made to add passive gills that will resist sudden fluctuations in speed inside the housing.

Descent profiles using traditional methods are unreliable compared to an ascent profile due to the turbulent mixing of air by the UAS while descending. While

our sensor housing can obtain reliable descent data that is within the sensors' uncertainty, some features in the data are still not fully captured, as evident from Figure 6.9. This would indicate that some turbulently mixed air is still passing through the housing inlet. Extending the housing even farther out would reduce the effect of mixed air further and would reveal more features in the observations. We note that any extension of the sensor housing would burden the flight controller as well and should be done according to the UAS's safety limit.

*Sensor Redundancy:* The sensor housing shields the sensor from external heat sources, but when located downstream from a heat source (such as the waste heat of the UAS), the effect is usually unavoidable. For the cases encountered in our experiments, the effect is not significant. If the UAS is equipped with sensors in the opposite arm, this could be solved in two ways: (1) a reorientation of the UAS (using data from an onboard anemometer) or (2) sensor fusion using the redundant data based on the wind/UAS speed and direction.

*UAS Safety Maneuvers:* The detection of turbulence and oscillations based on real-time data could allow the UAS to perform preprogrammed safe maneuvers to avoid a loss of control. This would allow for the safer operation of UASs at higher speeds, making the sampling process significantly faster.

*Correction of Measured Data:* The correction of sensor data can be complex without accurately characterizing the sensors. The sensor response time of the iMet XQ, for example, is based on the step response of the sensor while subjected to an oil bath. The step response information alone is not enough to correct for the dynamic response of the system. A robust method to characterize the dynamic response of the UAS/housing/sensor system would be needed to account for the deviation or to make any corrections since the system response time would be different for just the sensor vs. a sensor inside the housing *as flown* [29].

Another challenge in correcting the sensor data (such as the humidity) is the variability in response time based on temperature which should be taken into account for the correction routine. Additionally, as noted in previous literature, multirotors have a dispersion effect, and recirculating air can affect the measurement by changing the *actual* observation level. We suspect this will be more apparent in lower ascent/descent speeds as the air has a higher chance of being recirculated. These effects can be mitigated further by extending the air inlet even farther out from the body.

# Bibliography

[1] DJI Matrice 600 Pro. Available online: https://www.dji.com/matrice600-pro/info#specs. "(accessed on 2 May 2019)". 3.3

[2] Steven P Anderson and Mark F Baumgartner. Radiative heating errors in naturally ventilated air temperature measurements made from buoys. *Journal of Atmospheric and Oceanic Technology*, 15(1):157–173, 1998. 2.2, 3.1

[3] Lindsay Barbieri, Stephan T Kral, Sean CC Bailey, Amy E Frazier, Jamey D Jacob, Joachim Reuder, David Brus, Phillip B Chilson, Christopher Crick, Carrick Detweiler, et al. Intercomparison of small unmanned aircraft system (suas) measurements for atmospheric science during the lapse-rate campaign. *Sensors*, 19(9):2179, 2019. 2.4, 8

[4] Timothy Bonin, Phillip Chilson, Brett Zielke, and Evgeni Fedorovich. Observations of the early evening boundary-layer transition using a small unmanned aerial system. *Boundary-layer meteorology*, 146(1):119–132, 2013. 1

[5] GL Brown and MR Rebollo. A small, fast-response probe to measure composition of a binary gas mixture. *AIAA Journal*, 10(5):649–652, 1972. 1

[6] Michael S Buban, Temple R Lee, Edward J Dumas, C Bruce Baker, and Mark Heuer. Observations and numerical simulation of the effects of the 21 august

2017 north american total solar eclipse on surface conditions and atmospheric boundary-layer evolution. *Boundary-Layer Meteorology*, pages 1–14, 2019. 1

[7] Girish V Chowdhary, Sriram Srinivasan, and Eric N Johnson. Frequency domain method for real-time detection of oscillations. *Journal of Aerospace Computing, Information, and Communication*, 8(2):42–52, 2011. 7.3

[8] M de Podesta, R Underwood, L Bevilacqua, and S Bell. Air temperature measurement challenges in precision metrology. In *Journal of Physics: Conference Series*, volume 1065. IOP Publishing, 2018. 1, 2.1.2

[9] Michael de Podesta, Stephanie Bell, and Robin Underwood. Air temperature sensors: dependence of radiative errors on sensor diameter in precision metrology and meteorology. *Metrologia*, 55(2):229, 2018. 1, 2.1.2

[10] Jack Elston, Brian Argrow, Maciej Stachura, Doug Weibel, Dale Lawrence, and David Pope. Overview of small fixed-wing unmanned aircraft for meteorological sampling. *Journal of Atmospheric and Oceanic Technology*, 32(1):97–115, 2015. 1

[11] Jan W. Gooch. *Hagen-Poiseuille Equation*, pages 355–355. Springer New York, New York, NY, 2011. 4.2

[12] Colin Greatwood, Thomas Richardson, Jim Freer, Rick Thomas, A MacKenzie, Rebecca Brownlow, David Lowry, Rebecca Fisher, and Euan Nisbet. Atmospheric sampling on ascension island using multirotor uavs. *Sensors*, 17(6):1189, 2017. 1, 7.3

[13] Brian R Greene, Antonio R Segales, Tyler M Bell, Elizabeth A Pillar-Little, and Phillip B Chilson. Environmental and sensor integration influences

on temperature measurements by rotary-wing unmanned aircraft systems. *Sensors*, 19(6):1470, 2019. 1, 3.2, 3.2

[14] Brian R Greene, Antonio R Segales, Sean Waugh, Simon Duthoit, and Phillip B Chilson. Considerations for temperature sensor placement on rotary-wing unmanned aircraft systems. *Atmospheric Measurement Techniques*, 11(10):5519–5530, 2018. 1, 2.1.2, 2.2, 3.2, 4.1

[15] Benjamin L Hemingway, Amy E Frazier, Brian R Elbing, and Jamey D Jacob. Vertical sampling scales for atmospheric boundary layer measurements from small unmanned aircraft systems (suas). *Atmosphere*, 8(9):176, 2017. 1, 2.2

[16] Terrence F Hock and James L Franklin. The ncar gps dropwindsonde. *Bulletin of the American Meteorological Society*, 80(3):407–420, 1999. 1

[17] AAM Holtslag, EIF De Bruijn, and HL Pan. A high resolution air mass transformation model for short-range weather forecasting. *Monthly Weather Review*, 118(8):1561–1575, 1990. 1

[18] Adam L Houston, Brian Argrow, Jack Elston, Jamie Lahowetz, Eric W Frew, and Patrick C Kennedy. The collaborative colorado–nebraska unmanned aircraft system experiment. *Bulletin of the American Meteorological Society*, 93(1):39–54, 2012. 1

[19] Adam L Houston and Jason M Keeler. The impact of sensor response and airspeed on the representation of the convective boundary layer and airmass boundaries by small unmanned aircraft systems. *Journal of Atmospheric and Oceanic Technology*, 35(8):1687–1699, 2018. 1, 2.1.1, 2.2, 3.1, EXP 3, 6.4.3

[20] C. Houston, A.; Chilson, P.; Islam, A.; Shankar, A.; Greene, B.; Segales, A.; Detweiler. PTH Sensor Siting on Rotary-Wing UAS. In *In Proceedings of the 19th AMS Symposium on Meteorological Observation and Instrumentation*, Austin, TX, USA, jan 2018. AMS. (document), 1.1, 3.2, 6.3

[21] International Society for Atmospheric Research using Remotely Piloted Aircraft (ISARRA) 2018. Available online: https://isarra.colorado.edu/. (accessed on 25 February 2019). 1.1

[22] Ashraful Islam, Adam L Houston, Ajay Shankar, and Carrick Detweiler. Design and evaluation of sensor housing for boundary layer profiling using multirotors. *Sensors*, 19(11):2481, 2019. 1.1, 2.4

[23] Jamey Jacob, Phillip Chilson, Adam Houston, and Suzanne Smith. Considerations for atmospheric measurements with small unmanned aircraft systems. *Atmosphere*, 9(7):252, 2018. (document), 1, 1.1, 2.1, 2.2, 3.2

[24] Marius O Jonassen, Priit Tisler, Barbara Altstädter, Andreas Scholtz, Timo Vihma, Astrid Lampert, Gert König-Langlo, and Christof Lüpkes. Application of remotely piloted aircraft systems in observing the atmospheric boundary layer over antarctic sea ice in winter. *Polar Research*, 34(1):25651, 2015. 1

[25] Mark G Lawrence. The relationship between relative humidity and the dewpoint temperature in moist air: A simple conversion and applications. *Bulletin of the American Meteorological Society*, 86(2):225–234, 2005. 6.4.4

[26] Temple Lee, Michael Buban, Edward Dumas, and C Baker. On the use of rotary-wing aircraft to sample near-surface thermodynamic fields: Results from recent field campaigns. *Sensors*, 19(1):10, 2019. 1, 2.2, 3.2

[27] Temple R Lee, Michael Buban, Edward Dumas, and C Bruce Baker. A new technique to estimate sensible heat fluxes around micrometeorological towers using small unmanned aircraft systems. *Journal of Atmospheric and Oceanic Technology*, 34(9):2103–2112, 2017. 1, 2.2

[28] Temple R Lee, Edward James Dumas, Michael S Buban, C Bruce Baker, Jonathan Neuhaus, Mark Rogers, Nicole Chappelle, Casey Marwine, Maureen Swanson, Chris Amaral, et al. Improved sampling of the atmospheric boundary layer using small unmanned aircraft systems: results from the avon park experiment. 2019. 2.4

[29] John McCarthy. A method for correcting airborne temperature data for sensor response time. *Journal of Applied Meteorology*, 12(1):211–214, 1973. 2.1.1, 3.1, 5.1, 6.4, 8

[30] Mobile UAS Research Collaboratory (MURC). Available online: https://www.colorado.edu/iriss/content/equipment. (accessed on 27 February 2019). 3.3

[31] Peter Nolan, James Pinto, Javier González-Rocha, Anders Jensen, Christina Vezzi, Sean Bailey, Gijs de Boer, Constantin Diehl, Roger Laurence, Craig Powers, et al. Coordinated unmanned aircraft system (uas) and ground-based weather measurements to predict lagrangian coherent structures (lcss). *Sensors*, 18(12):4448, 2018. 1

[32] Odroid XU4. Available online: https://www.hardkernel.com/shop/odroid-xu4/. "(accessed on 25 February 2019)". 3.3

[33] Ross T Palomaki, Nathan T Rose, Michael van den Bossche, Thomas J Sherman, and Stephan FJ De Wekker. Wind estimation in the lower atmosphere us-

ing multirotor aircraft. *Journal of Atmospheric and Oceanic Technology*, 34(5):1183–1191, 2017. 1

[34] S Prudden, A Fisher, M Marino, A Mohamed, S Watkins, and G Wild. Measuring wind with small unmanned aircraft systems. *Journal of Wind Engineering and Industrial Aerodynamics*, 176:197–210, 2018. 1, 2.3

[35] S Prudden, A Fisher, A Mohamed, and S Watkins. A flying anemometer quadrotor: Part 1. In *proc International Micro Air Vehicle Conference (IMAV 2016)*, 2016. 1

[36] Robot Operating System (ROS). Available online: http://www.ros.org/. "(accessed on 25 February 2019)". 3.3

[37] AR Rodi and PA Spyers-Duran. Analysis of time response of airborne temperature sensors. *Journal of Applied Meteorology*, 11(3):554–556, 1972. 2.1.1

[38] Petra Seibert, Frank Beyrich, Sven-Erik Gryning, Sylvain Joffre, Alix Rasmussen, and Philippe Tercier. Review and intercomparison of operational methods for the determination of the mixing height. *Atmospheric environment*, 34(7):1001–1027, 2000. 1

[39] Patricia Ventura Diaz and Steven Yoon. High-fidelity computational aerodynamics of multi-rotor unmanned aerial vehicles. In *2018 AIAA Aerospace Sciences Meeting*, page 1266, 2018. 1, 2.3, 3.2

[40] Tommaso Villa, Felipe Gonzalez, Branka Miljievic, Zoran Ristovski, and Lidia Morawska. An overview of small unmanned aerial vehicles for air quality measurements: Present applications and future prospectives. *Sensors*, 16(7):1072, 2016. 1

[41] Tommaso Francesco Villa, Farhad Salimi, Kye Morton, Lidia Morawska, and Felipe Gonzalez. Development and validation of a uav based system for air pollution measurements. *Sensors*, 16(12):2202, 2016. 1, 1, 2.2, 2.3, 3.2

[42] Frank M White. Fluid mechanics, chapter 6, 1986. 4.2, 4.2

[43] Seokkwan Yoon, Patricia Ventura Diaz, D Douglas Boyd, William M Chan, and Colin R Theodore. Computational aerodynamic modeling of small quadcopter vehicles. *Proceedings of the AHS 73rd Annual Forum*, 5 2017. 1, 2.3, 3.2

## Appendix A

## Description of Flight Campaigns

### A.1    Oklahoma 2017

CLOUD-MAP Summer Field Campaigns in Oklahoma. 71 participants from four different universities participated in a five day long collaborative flight schedule to evaluate the performance of the systems developed and to collectively measure atmospheric phenomena. Experiments were conducted in three sites near Oklahoma State University: OSU Unmanned Aircraft Flight Station, Marena Mesonet site, Department of Energy Southern Great Plains Atmospheric Radiation Measurement site. More than 500 flights of fixed wing and multirotor UAS accumulated about 70 hours of flight time.

### A.2    Nebraska 2017

Measurements from the total solar eclipse in Wilber, Nebraska. Flights were conducted throughout the day in collaboration with Oklahoma State University. There was in total 26 Flights totalling up to 430 minutes in total flight time. Additionally, there were 16 NOAA radiosonde balloon launches to be used as reference for the measurements of multirotors.

Figure A.1: University of Nebraska-Lincoln Team' 2017



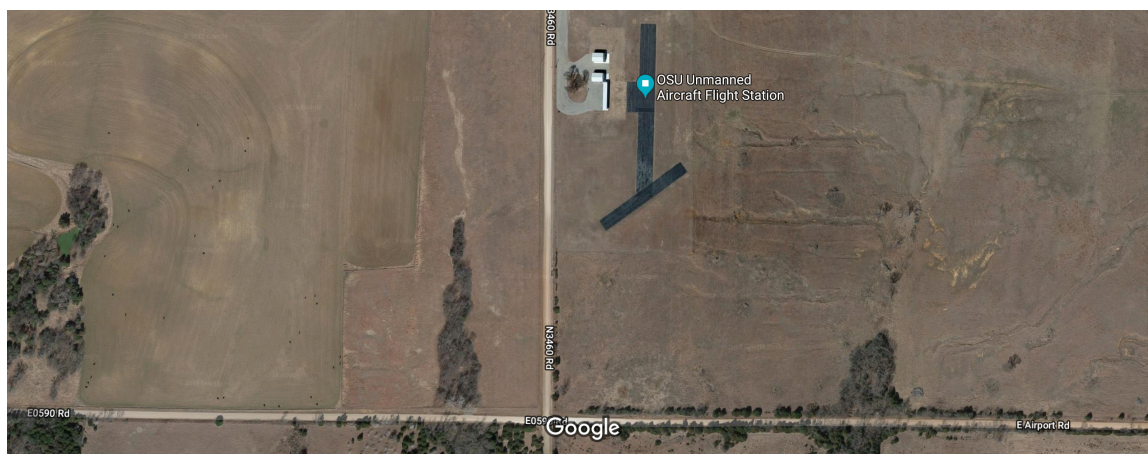Figure A.2: Teams participating from four university during CLOUDMAP flight campaign'2017.



Figure A.3: CLOUDMAP Flight Campaign Map, Oklahoma.

Figure A.4: University of Nebraska-Lincoln team for Solar Eclipse Campaign



Figure A.5: Multirotor in-flight collecting TH data seconds before the total solar eclipse.

Figure A.6: Launching of Radiosonde Balloon For TH data observations
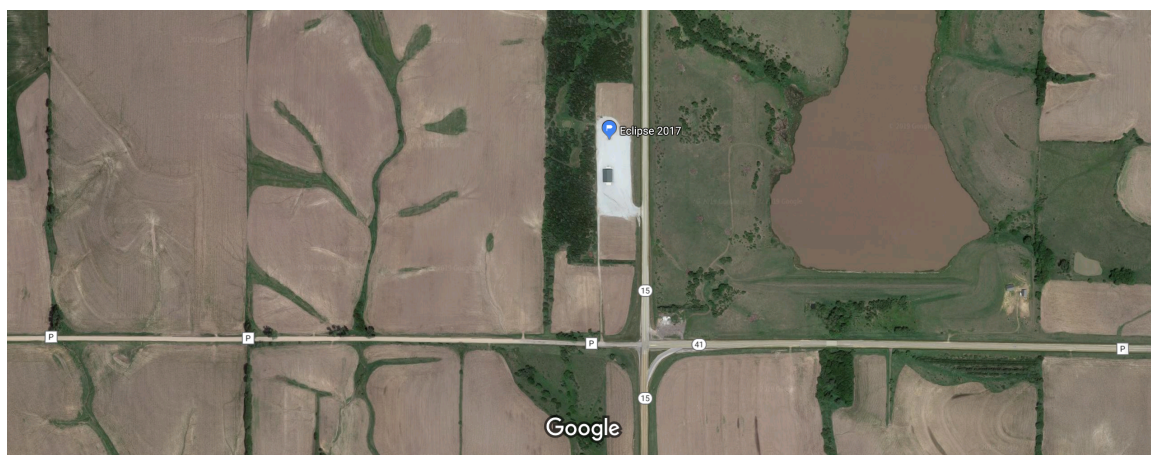


Figure A.7: Location of Solar eclipse campaign at Wilber, NE.

Figure A.8: University of Nebraska-Lincoln Team for LAPSE-RATE flight campgain.

## A.3   Colorado 2018

Lower Atmospheric Process Studies at Elevation - a Remotely-piloted Aircraft Team Experiment (LAPSE-RATE) flight campaign in San Luis Valley of Colorado during was organized by ISARRA conference committee. The San Luis Valley is a high-altitude valley surrounded by tall mountain peaks and is of great interest to atmospheric science community. The valley provides sampling opportunities related to boundary layer structure and development and its connection to complex terrain, convective initiation, aerosol properties, surface fluxes and more.

The field campaign spanned six days from 14-19th July, 2018. More than 100 participants from 13 university, government, and industry teams conducted flights with 35 UAS. Fixed and multirotor UASs combined, 1287 flights for about total of 260 hours were conducted by remote pilots.
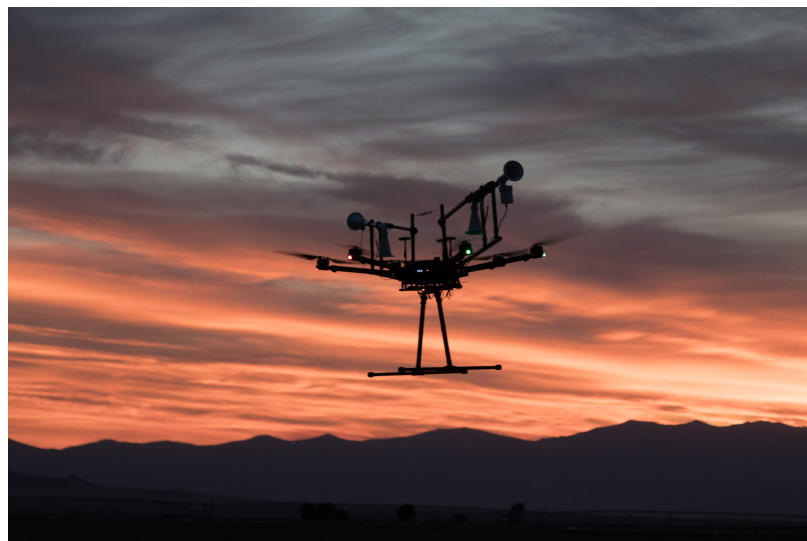
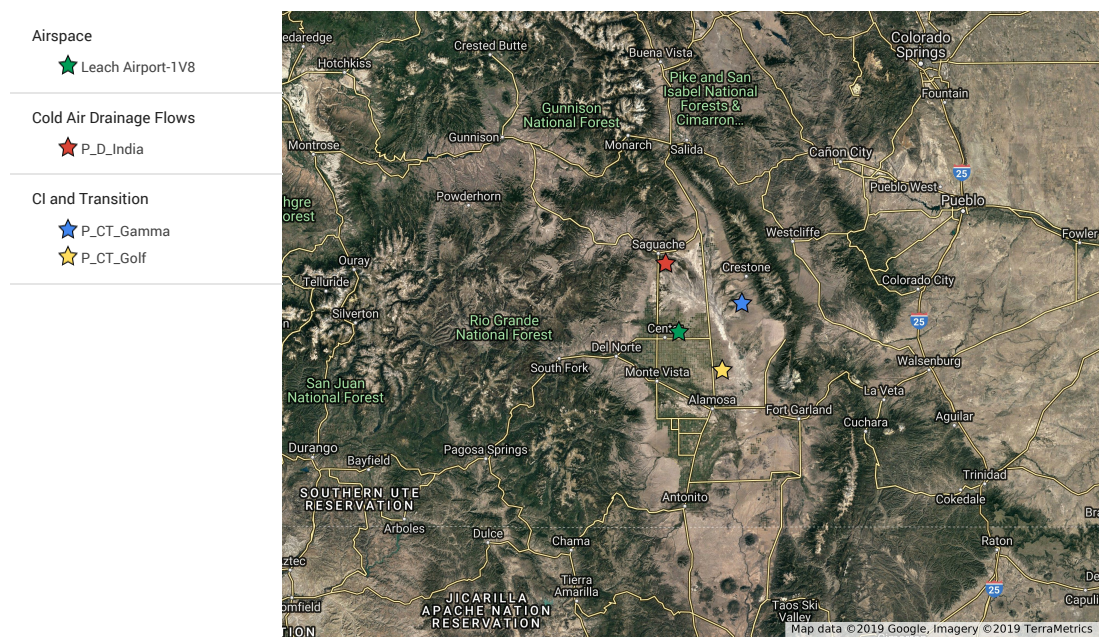Figure A.9: Multirotor inflight with the sensor housing to collect TH observations minutes before dawn.



Figure A.10: LAPSE-RATE'2018 flight week map.